Some Considerations for the Use of High-Resolution Mobile Radar Data in Tornado Intensity Determination

JEFFREY C. SNYDER

National Severe Storms Laboratory, Norman, Oklahoma

HOWARD B. BLUESTEIN

School of Meteorology, University of Oklahoma, Norman, Oklahoma

ABSTRACT

The increasing number of mobile Doppler radars used in field campaigns across the central United States has led to an increasing number of high-resolution radar datasets of strong tornadoes. There are more than a few instances in which the radar-measured radial velocities substantially exceed the estimated wind speeds associated with the enhanced Fujita (EF) scale rating assigned to a particular tornado. It is imperative, however, to understand what the radar data represent if one wants to compare radar observations to damage-based EF-scale estimates. A violent tornado observed by the rapid-scan, X-band, polarimetric mobile radar (RaXPol) on 31 May 2013 contained radar-relative radial velocities exceeding $135 \, \mathrm{m \, s}^{-1}$ in rural areas essentially devoid of structures from which damage ratings can be made. This case, along with others, serves as an excellent example of some of the complications that arise when comparing radar-estimated velocities with the criteria established in the EF scale. In addition, it is shown that data from polarimetric radars should reduce the variance of radar-relative radial velocity estimates within the debris field compared to data from single-polarization radars. Polarimetric radars can also be used to retrieve differential velocity, large magnitudes of which are spatially associated with large spectrum widths inside the polarimetric tornado debris signature in several datasets of intense tornadoes sampled by RaXPol.

1. Introduction

Radar has been a useful technology for the remote sensing of the atmosphere, particularly in areas that are hazardous or incompatible with in situ measurement platforms. Mobile radars seem to be particularly well suited for the observation of tornadoes owing to their ability to maximize spatial resolution (by reducing the distance between radar and tornado), and they can typically provide greater volumetric coverage near the ground compared to the coverage provided by most nonmobile radar systems (which typically sample tornadoes at greater ranges owing to their nonmobile nature). In the past decade, the number of mobile radars available for research has increased significantly; such platforms include the rapid-scan, X-band, polarimetric radar (RaXPol; Pazmany et al. 2013); the Mobile Weather Radar 2005 X-band phased-array radar (MWR-05XP; Bluestein et al. 2010); the Doppler on Wheels radars (DOWs; Wurman et al. 1997); the National Oceanic and Atmospheric Administration (NOAA) X-band polarimetric radar (NOXP or XERES; Melnikov et al. 2009); the Texas Tech University Ka-band radars (TTU-Ka; Weiss et al. 2011); and the Mobile, Alabama, X-band radar (MAX; Asefi-Najafabady et al. 2010). Rather uniquely, the antennas on RaXPol and MWR05XP are mounted on pedestals that can rotate up to $180° \, \mathrm{s}^{-1}$, producing a 360° sweep every 2 s; this increased temporal resolution is extremely useful when probing tornadoes and other rapidly changing phenomena.

The enhanced Fujita scale (EF scale; WSEC 2006) was developed to allow for more precise, accurate, and consistent assessments of tornado damage by expanding upon the original Fujita scale (Fujita 1981). Since there are wind speeds associated with the EF scale, damage assessors use the relevant damage indicators (DIs) and degree of damage (DoD) levels to arrive at an EF-scale

Corresponding author address: Jeffrey Snyder, National Severe Storms Laboratory/RRDD, 120 David L Boren Blvd., Norman, OK 73072.
E-mail: jeffrey.snyder@noaa.gov

category and, typically, an estimate of maximum wind speed. These ratings have been used for the study of tornado climatology across the United States and the correlation of environmental parameters with the occurrence of tornadoes of particular intensity (e.g., Kerr and Darkow 1996; Brooks and Doswell 2001; Brooks et al. 2003; Thompson et al. 2003, 2007; Brooks 2004; Mead and Thompson 2011; Garner 2012); the EF scale ratings are of interest to meteorologists as well as to those in many other industries (e.g., Womble and Smith 2009; Womble et al. 2009, 2011; Thampi et al. 2011; Kuligowski et al. 2013). For a general discussion on the history, development, advantages, and limitations of the EF scale, readers are referred to Doswell et al. (2009) and Edwards et al. (2013).

Since there are wind speeds provided with each category, it is tempting to use directly radial velocity[1] V_R data from high-resolution mobile radars in tornado intensity assessment. In fact, the EF-scale documents note that "portable Doppler radar should also be a part of the EF-scale process, either as a direct measurement, when available, or as a means of validating the wind speeds estimated by experts" (WSEC 2006, p. 14). In addition, the EF-scale rating for a tornado "should represent an estimate of the highest wind speed that occurred during the life cycle of the tornado" (WSEC 2006, p. 12). Assessing damage in the field can be extremely difficult, even if there are a sufficient number and "type" of DIs to allow one to estimate the maximum winds that occurred; for the more intense tornadoes, there may not be adequate DIs to assess confidently an upper bound to the estimated wind speed (e.g., Kuligowski et al. 2013). Since there often may be limited or no damage from tornadoes in rural areas relative to more populated locales, the frequency of violent tornadoes within tornado climatology is likely underrepresented. In a comparison between the Fujita- (F-) and EF-scale ratings determined by mobile radar observations and those assigned by damage assessment for more than 50 tornadoes produced by supercells across the central United States over

a ~10-yr period, Alexander and Wurman (2008) found that the official F- and EF-scale ratings determined by damage assessments often were lower than those that would be assigned based upon the wind speeds (within 500 m of the ground) observed by radar; the mode of the radar-determined EF-scale ratings of the tornadoes examined was EF2, whereas the mode of the ratings for the same tornadoes in the official database was EF0.

The damage produced by a particular tornado is not solely a function of the maximum wind speeds. The duration, variability, and full three-dimensional structure of winds of a particular magnitude, as well as debris loading (e.g., Gong et al. 2006; Lewellen et al. 2008), can modify the amount of damage produced by a tornado (e.g., Federal Emergency Management Agency 2012; Kuligowski et al. 2013). In an examination of visual, in situ, and radar observations of a tornado that occurred in Wyoming in 2009, Wurman et al. (2013) noted that very similar structures failed at significantly different wind speeds. The expert elicitation process by which wind speeds were estimated for a large variety of DoDs for each DI (and, therefore, by which damage to a particular DI was assigned an EF-scale rating) included participation by some of the leading experts in tornado damage assessment. However, estimating wind speeds necessary to produce certain damage can be extremely difficult since there are many complexities that may not have much to do with the actual speed, which can lead to great uncertainty in the damage–wind speed relationship. For example, the expected values provided by the expert panel for DoD 9 for the "institutional building" DI ranged from 120 to 230 mi h^{-1} (EF2–EF5; 53.6–102 m s^{-1}). The expert-provided expected values for other DoDs for other DIs spanned multiple EF-scale categories as well. Again, the widely varying estimates were produced by some of the leading experts in the field, so the spread in some of the wind estimates for some DoDs and DIs is indicative of the high uncertainty that accompanies relating damage to a 10-m AGL, 3-s-average wind speed used in the EF scale.

This paper highlights some ways in which V_R from radars may over- or underestimate EF-scale-equivalent wind speeds. *This paper is not an examination of the implementation of the EF scale or policies regarding the use of the EF scale by an organization.* At this time, there are still a limited number of high-resolution radar datasets of violent (EF4 and EF5) tornadoes, but that number is increasing, and a recent tornado that affected El Reno, Oklahoma, on 31 May 2013 and sampled by several high-resolution mobile radars [including the DOWs (Wurman et al. 2014) and RaXPol] provides an excellent example of the difficulties involved in relating

---

[1] The term "radial velocity" as used in radar observations of tornadoes can be ambiguous unless a reference frame is specified. For example, although radial velocity is often used by the radar community to describe the motion of scatterers toward or away from the radar, the speed of the radial component of the flow within a quasi-axisymmetric tornado is also commonly referred to as radial velocity. Throughout this paper, any mention of radial velocity is intended to refer to the motion toward or away from the radar, unless otherwise explicitly specified. Winds in a tornado-relative reference frame are usually described in a cylindrical coordinate system, and the tornado-relative radial velocity is herein referred to as u in keeping with precedent (e.g., Rotunno 1979; Fiedler and Rotunno 1986).

radar-retrieved wind speeds and the EF scale. Several examples of intense tornadoes sampled by RaXPol in 2011 and 2013 are presented as well; these cases are currently being analyzed in more detail and will be presented in later papers.

Given the considerations pertinent to the relationship between radar data and the EF scale, it is also important to address potential errors in the calculation of V_R. Although such errors are discussed elsewhere (e.g., Doviak and Zrnić 1993, hereafter DZ93), lesser attention has been provided to a couple of unique advantages of polarimetric radars. The impact of debris within tornadoes on the statistical accuracy of V_R measurements from high-resolution mobile radars has been discussed relatively little in the formal literature, although the effect of debris in broadening the Doppler spectrum has been discussed insofar as it concerns lower-resolution observations from fixed-location radars. The purposes of this paper are to 1) review the meaning of a V_R measurement relative to a 3-s, 10 m AGL wind speed standard, 2) discuss special considerations that must be made when comparing radar observations to such a standard, 3) present some observations of intense tornadoes observed at close range collected by RaXPol in 2011 and 2013, 4) examine the use of polarimetric velocity estimates within the debris cloud, and 5) evaluate the use of radar-relative differential radial velocity (V_D; the difference between V_R calculated separately using data from two orthogonally polarized beams). We hope this paper is useful to operational meteorologists and others who are involved in tornado rating assessments.

2. Radar observations and the "enhanced Fujita scale"

a. What the observations represent

It is useful to reiterate what the commonly used V_R data from Doppler radars actually represent. The V_R estimates from weather radars represent the reflectivity-weighted average velocity of all scatterers within a resolution volume during a given integration period (i.e., dwell time) toward or away from the radar. Each of the five subsections discuss the relationship they have with the standard EF-scale wind speeds (i.e., 3-s wind gust at 10 m AGL) will be noted.

1) V_R ESTIMATES

The calculation of V_R for a given radar volume is based upon a finite number of samples and often requires assumptions to be made about the shape and distribution of the received power spectrum. A method of calculating V_R based upon the change in received

phase between consecutive pulses [i.e., pulse-pair processing (PPP)] is used by RaXPol and many other weather radars; the accuracy of the estimate using this technique is sensitive to, among other things, the number of samples available, the independence of each sample (often related to the spectrum width σ_v), and the signal-to-noise ratio (SNR). More discussion of some factors that affect the quality of the estimate is provided in section 4.

2) REFLECTIVITY-WEIGHTED AVERAGE VELOCITY

Measurements of V_R will be biased toward the largest and most abundant scatterers within the resolution volume. Unfortunately, the particular distribution (size, number, and type) of scatterers within a radar volume is unknown in nearly all cases. However, since there can be very large accelerations in strong tornadoes, the varying density, shape, and mass of hydrometeors and debris, and thus differing drag characteristics, within a resolution volume may result in scatterer velocities that deviate significantly from the local air velocities owing to such effects as centrifuging and gravitational sedimentation (e.g., Lewellen et al. 2008). Simulating the effects of debris on tornado characteristics using a numerical model, Lewellen et al. (2008) reported that the difference between air velocity and the velocity of simulated debris (sand) was largest for the largest simulated sand sizes (2 mm). In addition, the *peak* debris velocities within the tornadoes were lower than the *peak* air velocities, although the deviation of the local debris velocity from the local air velocity varied in time and space and by debris characteristics (e.g., the outward-directed radial component of the debris can appreciably exceed that of the air near the upper-core region owing to debris centrifuging). Although the specific difference between scatterer velocity and air velocity in any given tornado is unknown, it is reasonable to suggest that, at least above the very shallow tornado inflow layer, the peak air velocities within a tornado will exceed the peak velocity of scatterers; the peak magnitude of V_R measured by radar is likely to be lower than the peak V_R if only the air motion were sampled.

3) WITHIN A RESOLUTION VOLUME

Although some characteristics of radar systems can be modified to allow for increased spatial resolution (e.g., decreasing the pulse length), the illuminated radar volume produced by current mobile radars becomes larger with increasing range (on account of beam spreading) and typically is 60–300 m in the radial direction (corresponding to a range resolution of 30–150 m). At a range of 5 km, the resolution volume produced from a parabolic

antenna with a 1° 3-dB (half-power) beamwidth[2] has a horizontal cross section of approximately 87 m, which increases to ~260 and ~525 m at ranges of 15 and 30 km, respectively. For a pulse with a 30-m range resolution, neglecting areas beyond the half-power beamwidth, the resolution volume is approximately 1.8×10^5, 1.6×10^6, and $6.5 \times 10^6 \, \text{m}^3$ in size at 5-, 15-, and 30-km range, respectively. The actual peak wind speeds within this resolution volume may substantially exceed the 'mean' velocity of scatterers within the resolution volume as a result of what may be a large radar volume. This can become more complicated if the distribution of scatterers within a resolution volume is not homogeneous or random; one cannot then assume that the measured V_R is valid for the resolution volume symmetric about the beam center if there are significant gradients in scatterers within a resolution volume. For example, non-homogeneous scatterer distributions may be correlated with nonhomogeneous air velocity distributions (Lewellen et al. 2008). Regardless, the scatterers most influencing V_R may be located appreciably away from beam center (i.e., either nearer to or farther from ground level). In all cases, the resolution volume is many times larger than "infinitesimally small," and this spatial averaging is likely to contribute to V_R being lower than the EF-scale-equivalent wind speeds.

4) During a given integration period

Most radars used for studying severe convective storms and tornadoes in the United States are pulsed radars in which a series of pulses are averaged over a given dwell time to calculate the radar quantities. The statistical accuracy of the measurements tends to increase with increasing dwell time (i.e., more samples are used to calculate common radar quantities and enhance the estimates). Techniques such as frequency hopping, which is used in RaXPol, can reduce the dwell time by decreasing the correlation between subsequent pulse groups, so that the antenna rotation rate and effective azimuthal resolution can be increased. In the rapid-scan cases collected by RaXPol, radials are calculated every 1° in azimuth, which, when the pedestal is rotating at $180° \, \text{s}^{-1}$, means that the samples used to calculate radar quantities for a given radial are collected over a ~5.6 × 10^{-3} s period; the V_R data are essentially "instantaneous" observations. Since the EF-scale wind speeds pertain to 3-s

wind gusts, the extremely short integration period used by most weather radars is likely to lead to V_R data that are higher than EF-scale-equivalent winds. In addition, the dwell time and antenna rotation rate determine the additional reduction in azimuthal resolution that occurs; the effective beamwidth accounts for antenna rotation during the integration period and is ~2° when an antenna with a 1° 3-dB beamwidth is rotated 1° during the integration period. As such, the "effective" resolution volume is considerably larger than a pulse resolution volume.

5) Toward or away from the radar

Traditional Doppler weather radars are only able to measure the component of the flow toward or away from the radar; the radar cannot measure the cross-beam component (i.e., in azimuth or in the vertical). The flow around and within tornadoes can be extremely complex and asymmetric. In addition, high-resolution tornado-scale simulations [e.g., Lewellen et al. (2002); Xia et al. (2003); Lewellen and Lewellen (2007)] suggest that the vertical velocity within tornadoes may be extremely high and may exceed the horizontal velocity at times; if the elevation angle is not 0°, there will be a contribution within the measured V_R from the vertical velocity. This may be problematic because the EF scale primarily considers only the horizontal wind. The ability of structures and other DIs to withstand forces associated with winds of a particular intensity may be significantly modified if the velocity vector has a substantial vertical component. The "radial component only" nature of V_R estimates from Doppler radars has an unknown effect on the applicability of V_R data to EF-scale-equivalent winds.

b. Considerations

Owing to the need to maintain some pulse-to-pulse signal correlation (necessary to calculate V_R), the general desire to maximize unambiguous range, minimize second-trip contamination, and maximize the speed of data collection, the maximum unambiguous velocity V_a for a given scanning strategy in an X-band radar may be much lower than the peak V_R within a tornado. Velocity dealiasing or "unfolding" is necessary in such cases. There may be extremely large gradients in V_R within tornadoes for typical dimensions of the resolution volume, so dealiasing can, at times, be described as an "art." In general, the strategy is to make dealiasing-related decisions that minimize the amount of high-frequency, along-radial divergence–convergence; additional temporal and spatial continuity checks are often warranted. While a staggered pulse repetition time (staggered PRT) strategy can increase V_a several fold, the subsequent increase in the variance of V_R increases the probability

---

[2] The 3-dB (down) beamwidth is the angular width of the radar beam in which the power density is no less than 3 dB reduced from its peak value within the main lobe. Likewise, the 10-dB beamwidth is determined by the angular width at which the power density within the main lobe is 10 dB down from its peak.

that erroneously high V_R will be calculated. For most RaXPol datasets, a single PRT was used, although staggered PRT was used on several days. In the latter cases, the V_R from the staggered PRT are used to help dealias the lower-variance V_R estimates from one of the individual pulse-pair estimates.

Additional data quality checks may be performed. For example, the power-based RaXPol measurements are thresholded on SNR < 0 dB. Normalized coherent power (NCP) is inversely proportional to σ_v[3] and has been used to remove V_R estimates at range gates for which coherency is questionable (e.g., Wurman et al. 2007); V_R presented in this paper include gates only for which NCP > 0.2. *To increase consistency between observations collected by different mobile radars and reported in the formal literature, it is beneficial to develop a standard by which observations can be reported and compared between radars as the number of tornado datasets increases.* Such relevant data may include estimated beam volume dimensions, estimated beam height above radar level, any signal quality thresholds applied (e.g., based upon NCP and SNR), the number of samples and the equations/methods used to calculate the moments, the SNR of the reported range gates, and any additional postprocessing that may have been applied to the data.

Whereas the wind speeds assigned to each EF-scale category are valid at 10 m AGL, radar observations generally come from considerably above 10 m AGL. The exact height of the centerline of the radar beam is almost always unknown since the exact profile of atmospheric refractivity is unknown. In addition, partial beam blockage downradial of ground clutter targets can be a significant problem for mobile radars since the mounting height of the antenna above ground is limited. The detrimental effect of ground clutter on near-surface radar observations is prominent in areas in which there are many trees or structures. In all cases, the shape of the radar-illuminated volume may be modified by ground clutter, adding to the complexity of estimating the height and location of the scatterers being sampled.

The above considerations may account for some of the differences between observed near-surface tornadic flow patterns determined from theoretical and laboratory studies and those inferred from radar observations of tornadoes, and these differences likely are indications that part of the flow within tornadoes is not being sampled sufficiently by radars. In general, modeling results [e.g., see Rotunno (2013) for a review of tornado-scale modeling and theory] and photographic observations

[e.g., treefall patterns—Beck and Dotzek (2010); Karstens et al. (2013); Fig. 1] indicate that there can be very strong tornado-relative radial flow (i.e., high magnitude of u) within the tornado inflow layer near the ground, and numerical simulations generally indicate that the peak in tornado-relative tangential wind speeds occurs above the peak u in the tornado inflow layer (e.g., Lewellen et al. 2008). There are an extremely limited number of radar datasets, however, that capture substantial tornado-relative radial convergence within the tornado boundary layer (e.g., Kosiba and Wurman 2013); the vast majority of radar observations of tornadoes show tornado-relative azimuthal flow dominating radial flow. There are likely at least two reasons for the lack of observed radial convergence in most radar datasets of tornadoes: the tornado inflow layer may be very shallow [e.g., <15 m AGL in Kosiba and Wurman (2013); <10 m AGL in the simulations presented in Lewellen et al. (2008)] and significant debris centrifuging may bias radar observations (e.g., Bluestein et al. 1993; Dowell et al. 2005; Wakimoto et al. 2012; Nolan 2013).

With beam spreading and partial beam blockage from ground clutter, illuminated volumes produced by most weather radars typically encompass a large area above the shallow near-surface tornado inflow layer when the radar is more than a couple of kilometers from the tornado. To mitigate this problem, radars often need to be very close to tornadoes with limited ground clutter between the tornado and radar. A radar with a much narrower beamwidth, such as the University of Massachusetts (UMass) W-band radar (e.g., Bluestein and Pazmany 2000; Bluestein et al. 2007b) or TTU-Ka (Weiss et al. 2011), or a pulsed Doppler lidar such as the Truck-Mounted Wind-Observing Lidar Facility (TWOLF; Bluestein et al. 2014), can be used to observe flow very near the ground, which alleviates some of the ground clutter problems. However, a lidar typically cannot collect data through precipitation, condensed water vapor (e.g., tornado condensation funnels), tornado debris/dust, and other visually opaque media, and W-band and Ka-band radars are more susceptible than X-band radars to severe attenuation, reducing the probability of sampling a tornado in its full horizontal extent.

Considering the difficulties in collecting near-ground observations, there are only a limited number of datasets from which comparisons between V_R measurements and near-ground (<10 m) observations can be made. Bluestein et al. (2007b; see their Fig. 15), presenting near-ground observations from a W-band radar, found that wind speeds decreased approximately 20% from ~20 m AGL to "near the ground." Wurman et al. (2013), using in situ anemometer observations collocated beneath high-resolution observations collected by

---

[3] Equation (6.27) in DZ93 is used to calculate σ_v from RaXPol data.
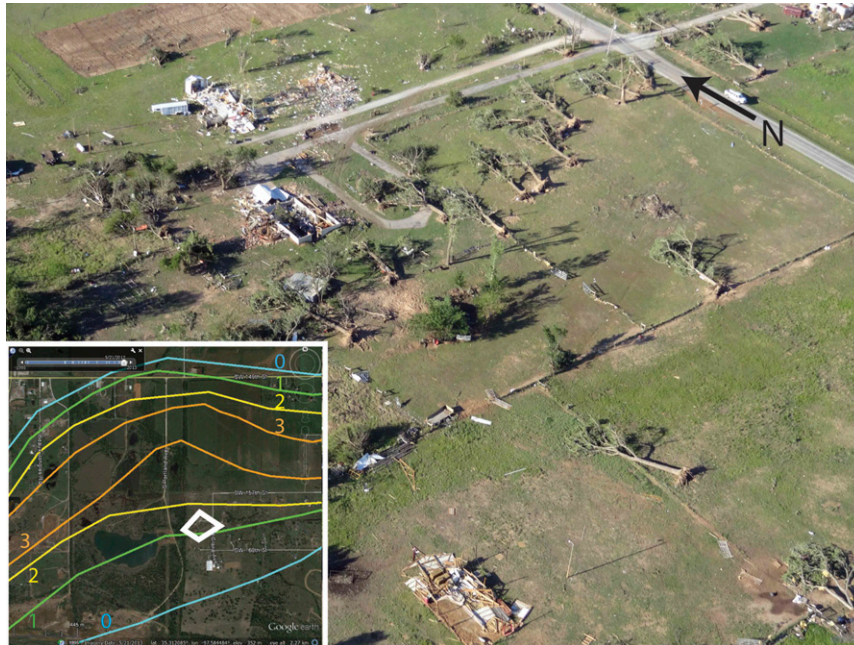
FIG. 1. An aerial photograph of damage from the 20 May 2013 EF5-rated tornado southwest of Moore, OK. The center of the tornado passed approximately 750 m north of this location. North is to the top left; the north arrow that has been superimposed over the top-right part of the image is approximately 30 m in length when projected onto the ground. Nearly all trees were felled to the north, implying strong southerly winds (i.e., oriented radially inward in a tornado-relative reference frame). (inset) The EF-scale contours provided by the National Weather Service Forecast Office in Norman, OK (NWSFO OUN); north is toward the top in the inset image. The white box in the inset image marks the approximate location of the photograph. [Photograph courtesy H. Bluestein.]

a DOW mobile radar, concluded that the most intense winds observed during the time of collocated data collection within a 2009 Wyoming tornado likely occurred below 30 m AGL, similar to the data presented in Wurman and Alexander (2005) that reveal peak winds with a different tornado occurred <50 m AGL. Kosiba and Wurman (2013) showed that peak winds occurred ~5 m AGL within a tornado observed by a DOW in Kansas in 2012. Wurman et al. (2007) showed that the vertical profile of wind speeds in two tornadoes observed at close range were inconsistent and quite unsteady below 100 m AGL. In nearly all of these cases, the winds observed above 50 m AGL were not greater than (and, in some cases, were appreciably lower than) winds that were measured very near the ground (<10 m AGL). As such, although there are significant questions about what radar measurements collected above 50 m AGL may reveal about 10 m AGL winds relevant to the EF scale, observations, limited as they may be, along with theory and numerical simulations indicate that the EF-scale-equivalent wind speeds in a "typical" tornado are likely to be no less than the 50+ m AGL winds that may be observed by radar. The sample size of all near-ground

radar datasets of tornadoes is very limited, however, and variations from one tornado to another (and through the lifetime of a tornado) are likely.

3. Some low-level wind observations in violent tornadoes observed by RaXPol

a. 31 May 2013

A series of tornadoes moved across central Oklahoma during the afternoon and evening of 31 May 2013 as an intense supercell traversed the Oklahoma City, Oklahoma, area. This particular dataset provides an excellent opportunity to examine some of the aforementioned potential complications when reconciling mobile radar measurements with the EF scale. Refer to the appendix for a very brief primer on the radar quantities that are used in this paper.

RaXPol deployed 7 times through the event, and the data presented herein were collected at the second and third deployment locations (marked D2 and D3 in Fig. 2). Digital Elevation Model data from National Elevation Dataset available from the U.S. Geological Survey with ⅓-arc-s resolution (~10 m horizontal and
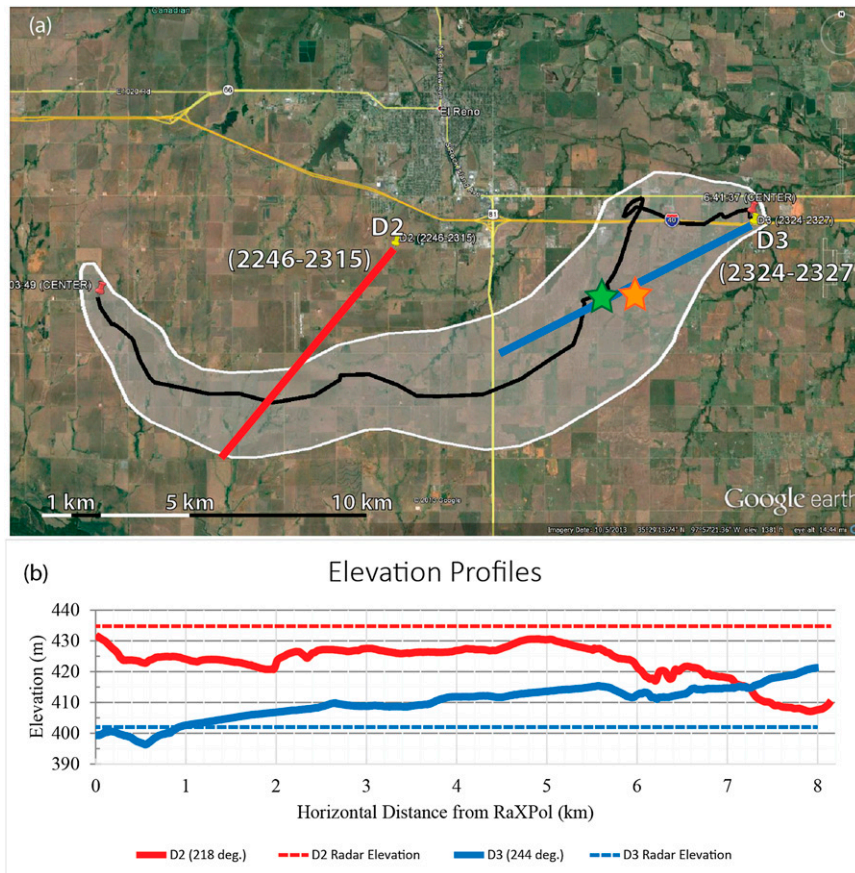
FIG. 2. (a) A map of RaXPol deployments during the El Reno tornado on 31 May 2013. The white enclosed area marks the approximate area of the tornado as determined by NWSFO OUN using radar and damage survey information. The black line within the white swath in (a) marks the approximate center of the tornado track. (b) The red and blue lines in (a) mark the profiles along which the ground elevations colored in red and blue, respectively, are plotted. The dashed horizontal lines in (b) mark the radar heights at the second (red; D2) and third (blue; D3) deployment locations (i.e., the approximate height of the 0.0°-elevation angle beam if the radar were perfectly level). The green and orange stars in (a) are locations of photographs presented in Figs. 11a,b. Elevation data in (b) are extracted from $\frac{1}{3}$-arc-s resolution (~10-m horizontal resolution) Digital Elevation Model data from the U.S. Geological Survey's (USGS) National Elevation Dataset; the root-mean-square error of the elevation data is approximately 2.4 m per the USGS.

1 m vertical with a root-mean-square error of ~2.4 m) have been used to examine the elevation of the ground where the tornado occurred; the elevation profiles for two selected azimuths from D2 and D3 illustrate some of the variability of the terrain in the vicinity of the tornado (Fig. 2b). In both ~8-km-long profiles, the ground elevation changes over a ~25-m range, which is important to keep in mind when examining the boresight-aligned estimated beam height relative to the 10 m AGL height (which subsequently becomes a function of range and azimuth given nonuniform elevation). However, compared to many mobile radar deployments, the terrain was relatively flat and open.

During D2, RaXPol observed the genesis and intensification of an intense, multiple-vortex tornado southeast of El Reno (Fig. 3). Ground clutter targets from D2 were relatively sparse in the direction of the tornado. The structure of the supercell and hook echo sampled by RaXPol can be seen in Fig. 4. At this time, RaXPol was collecting rapid-scan radar volumes consisting of seven 360° scans at elevation angles of 0°–5° every 1° (with two consecutive 0° scans) while the antenna rotated at ~180° s^{-1}. Range resolution was 30 m during most of the time the tornado was occurring, with oversampled gates every 15 m. A number of notable features are evident in the 5°-elevation scan: a weak
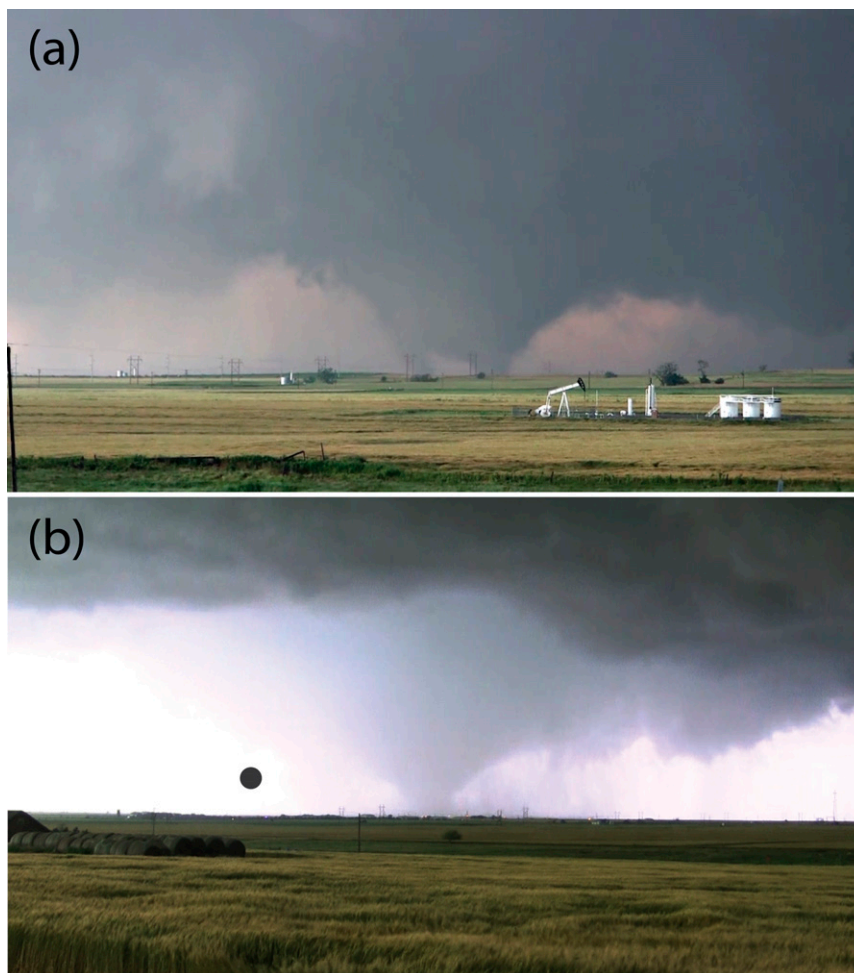
FIG. 3. Photographs of the tornado across rural areas of southwestern El Reno on 31 May 2013 taken at approximately (a) 2307 UTC (view to the west-southwest) and (b) 2314 UTC (view to the southwest). The multivortex structure of the tornado is evident in (a). A view of the relatively clutter-free and flat horizon can be seen in (b); a lightning strike makes the tornado in (b) much more apparent than it was moments before and after this image as copious amounts of precipitation surrounded the tornado. The black circle in (b) represents the approximate 3-dB beamwidth at 6-km range [near the tornado in (b)]. Both photographs were taken at the second deployment location (D2; Fig. 2a). [Photographs courtesy of J. Snyder.]

echo eye in Z_H (Fig. 4a) associated with the tornado, a possible low-reflectivity ribbon (e.g., Snyder et al. 2013), and a polarimetric tornado debris signature (PTDS; e.g., Ryzhkov et al. 2005) most evident in copolar cross-correlation coefficient (ρ_{hv};[4] Fig. 4d) and Z_{DR} (Fig. 4b). At 0°-elevation angle, the tornado is associated with a local maximum in Z_H, and peak V_R is approximately 86 m s^{-1}. The boresight-aligned theoretical

beam height at the range of the tornado, after including the platform pitch ($-0.42°$) and roll ($0.03°$), is approximately -55 m above radar level (ARL) or approximately -30 m AGL when including the height of the radar antenna above ground and the ground-elevation difference between D2 and the tornado. Obviously, data were not collected below ground level: the bottom part of the radar beam intercepted the ground, leaving only the top part of the beam illuminated. Owing to multipath scattering and otherwise unknown interactions as part of the radar beam intercepted the ground [e.g., see Beamer (1970); though the significantly different frequencies and distances examined therein compared to the observations presented herein complicate the

---

[4] In most uses of polarimetric radar data in meteorology, the relevant parameter typically is the magnitude of the copolar cross-correlation coefficient at lag 0 [i.e., $|\rho_{hv}(0)|$]. In this paper, all references to this quantity will be referred to solely by ρ_{hv}.
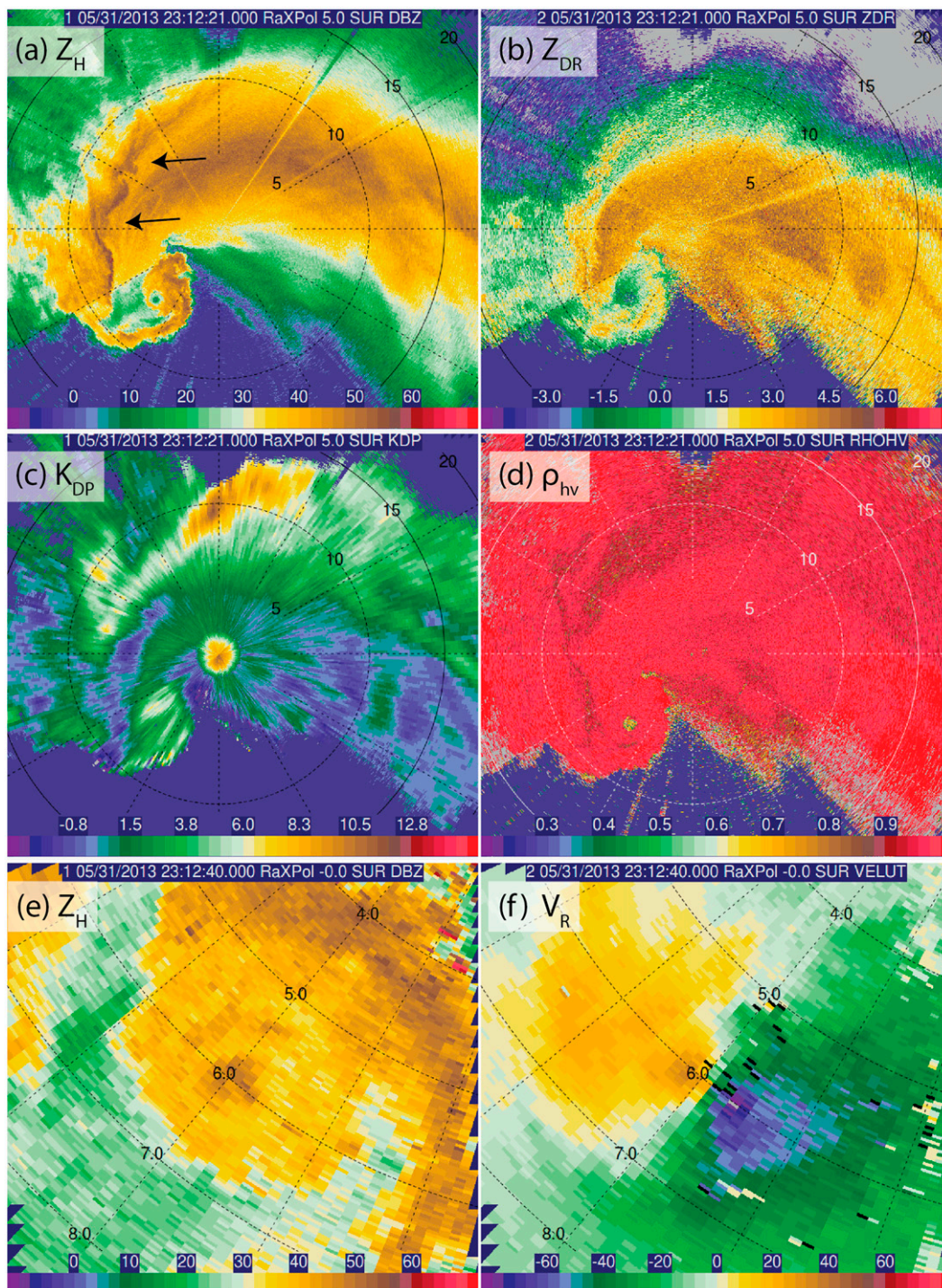
FIG. 4. RaXPol (a) Z_H (dBZ), (b) Z_{DR} (dB), (c) K_{DP} (° km^{-1}), and (d) ρ_{hv} from deployment location D2 in southwestern El Reno at 2312:21 UTC at a radar-relative elevation angle of 5.0°. A polarimetric tornado debris signature is evident in (b) and (d), and a possible low-reflectivity ribbon is noted [in black arrows in (a)] as well. Graphics of (e) Z_H and (f) V_R (gates with NCP < 0.2 are black) from 2312:40 UTC at a radar-relative elevation angle of 0.0° capture data much nearer the ground than shown in (a)–(d); the antenna boresight-aligned estimated beam center is approximately −55 m above radar level (i.e., only the top of the beam is illuminated owing to significant partial beam blockage from the ground). The strongest inbound velocities are −85.8 m s^{-1} in (f). Data in (e) and (f) are more ''speckly'' compared to data at higher-elevation angles on account of ground clutter and partial beam blockage.

application of those results to the current work], the illumination pattern of the beam was likely very complex at very low-elevation angles. Since it is impossible to assign a single height to a particular range gate under very atypical beam illumination patterns, beam heights provided in this paper, unless otherwise specified, are provided relative to antenna boresight. Readers should remember, however, that the actual height of scatterers contributing most to a volume is unknown and may deviate significantly from beam boresight.

Since the radar was 6 km from the tornado, our ability to collect very high-resolution data near ground level was limited. Although the boresight-aligned estimated beam height may have been very low with a radar-relative elevation angle of 0° and with limited clutter and terrain variability, the 3-dB cross-sectional width of the beam at 6-km range was ∼105 m. Nonetheless, vertical profiles of the observed maximum magnitude of V_R, collected shortly before RaXPol departed D2 (Fig. 5), show that the greatest V_R occurred at the lowest height of data collection during each volume. Owing to the large beam size at 6-km range, the radar is not resolving the tornado boundary layer, although scatterers within the tornado boundary layer may be contributing to the total signal measured by the radar. Although this is nearly an ideal deployment location given the situation, it is very difficult to collect very near-ground data from a range of more than a kilometer or two. At very low-elevation angles, there is an unknown contribution from potential forward scattering of the radar beam off the ground (J. Wurman 2014, personal communication). However, in an extremely simple case of mirrorlike "reflection" off a flat surface, radar volumes collected at increasingly lower elevation angles below 0° should be sampling scatterers at increasingly higher altitudes (i.e., the "lower" the antenna points, the higher the "reflected" beam gets), indicating that there will be some symmetry of the data about the 0°–0.5°-elevation angle; such symmetry does not appear to have been observed in this dataset. Ground interception of the beam very significantly biases power-based measurements (e.g., Z_H), but, as is observed in cases of partial beam blockage and signal attenuation, phase information necessary for V_R is much more immune to such effects and is generally preserved even where much of the signal has been lost.

The tornado grew to an extremely large size by the time RaXPol was collecting data at D3 (Figs. 6–12). When the radar was scanning again at D3, the tornado was located ∼5 km to the southwest (Fig. 7). For safety reasons, data collection at D3 lasted only approximately
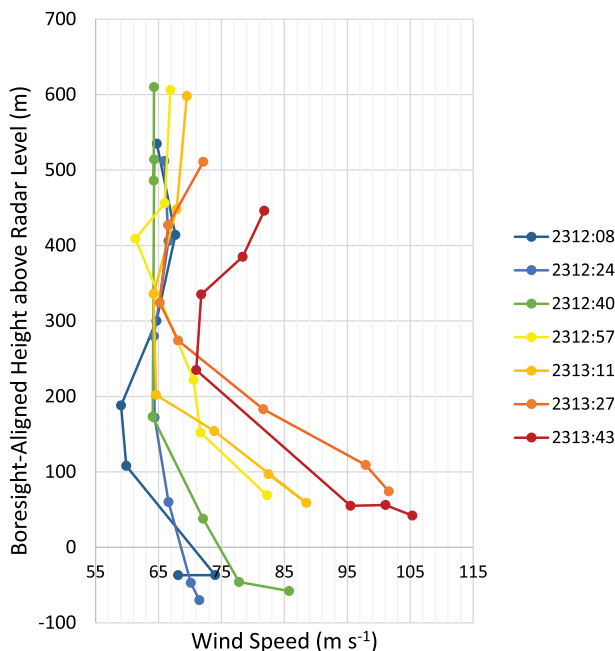

FIG. 5. The vertical profiles of maximum magnitude of inbound V_R (m s^{-1}) for volumes collected between 2312:08 and 2313:43 UTC at D2. Each volume provided seven scans in total: two from an elevation angle of 0.0° and one from each elevation angle of 1.0°, 2.0°, 3.0°, 4.0°, and 5.0°. In anticipation of needing to relocate the radar truck for the next deployment, the truck was unleveled after the 2312:40 UTC volume, which resulted in a loss of data below 50 m ARL. In addition, without the leveling system employed after 2312:40 UTC, the pitch and roll of the radar truck (and thus the estimated beam heights) were considerably more variable owing primarily to buffeting from the wind.

2 min. The period of data collection at D3 included the time during which the tornado appeared to transition from a primarily single-vortex structure to a multiple-vortex structure (e.g., Figs. 8 and 9). Since the tornado was closer to the radar at D3 than it was during D2, the data collected at D3 are of considerably higher resolution and contain more data near the ground. Although the center of the beam from the radar-relative 0°-elevation angle as determined by the antenna boresight is approximately −50 m at 4-km range after accounting for nonzero pitch and roll, the top extent of the radar volume as determined by the 3- and 10-dB beamwidths (1.0° and ∼1.8°, respectively) are −15 m and +12 m AGL, respectively. The vertical distribution of scatterers near the ground is unknown, but energy density decreasing rapidly beyond the 10-dB beamwidth (i.e., greater than ∼0.9° above antenna boresight) increases the probability that scatterers affected by very near-ground winds were also sampled by the top part of the main radiation lobe.

FIG. 6. Photographs of the 31 May 2013 El Reno tornado (a),(b) at 2325 UTC from RaXPol's third deployment location (D3) looking southwestward toward the tornado and (c) near 2326 UTC from a storm chaser (G. Rhoden) looking westward. The red circles near the left edges of (a) and (b) represent the approximate theoretical 3-dB beamwidth at 2.5-km range. The white arrow in (c) points to RaXPol as it was scanning. The highly slanted condensation funnel along the right side of (a) and (b) falls entirely within the 3-dB beamwidth. [Photograph in (a) courtesy of J. Snyder, photograph in (b) courtesy of H. Bluestein, and photograph in (c) courtesy of G. Rhoden.]

Shortly after 2325 UTC, V_R exceeding $130 \, \mathrm{m \, s^{-1}}$ (e.g., Fig. 8) was measured when the boresight-aligned theoretical beam height was <10 m AGL, and these particularly high winds were sampled in at least one subvortex that moved at $\sim 78 \, \mathrm{m \, s^{-1}}$ (Fig. 9). Although the maximum V_R associated with this particular subvortex ($135.0 \, \mathrm{m \, s^{-1}}$) was sampled only at higher-elevation angles (4°–5°), this may be attributable more to the time than to the height of the observation in that the highest winds were sampled when the subvortices were moving directly toward the radar, which happened to be when the radar was scanning at higher-elevation angles. As a result of the high translational speed of the subvortices, the highest winds were only over a particular area for a very short time.[5]

Since RaXPol collected a 360° sweep every 2 s, two consecutive scans can be averaged to yield an estimated

---

[5] No geometric corrections to account for the difference between the translation vector of the tornado (or a subvortex) and the radar-relative radial vector have been made to the estimates presented in this paper. As such, minor changes in the relative translational vector of a subvortex would be expected to result in a reduction in measured V_R from geometry alone.
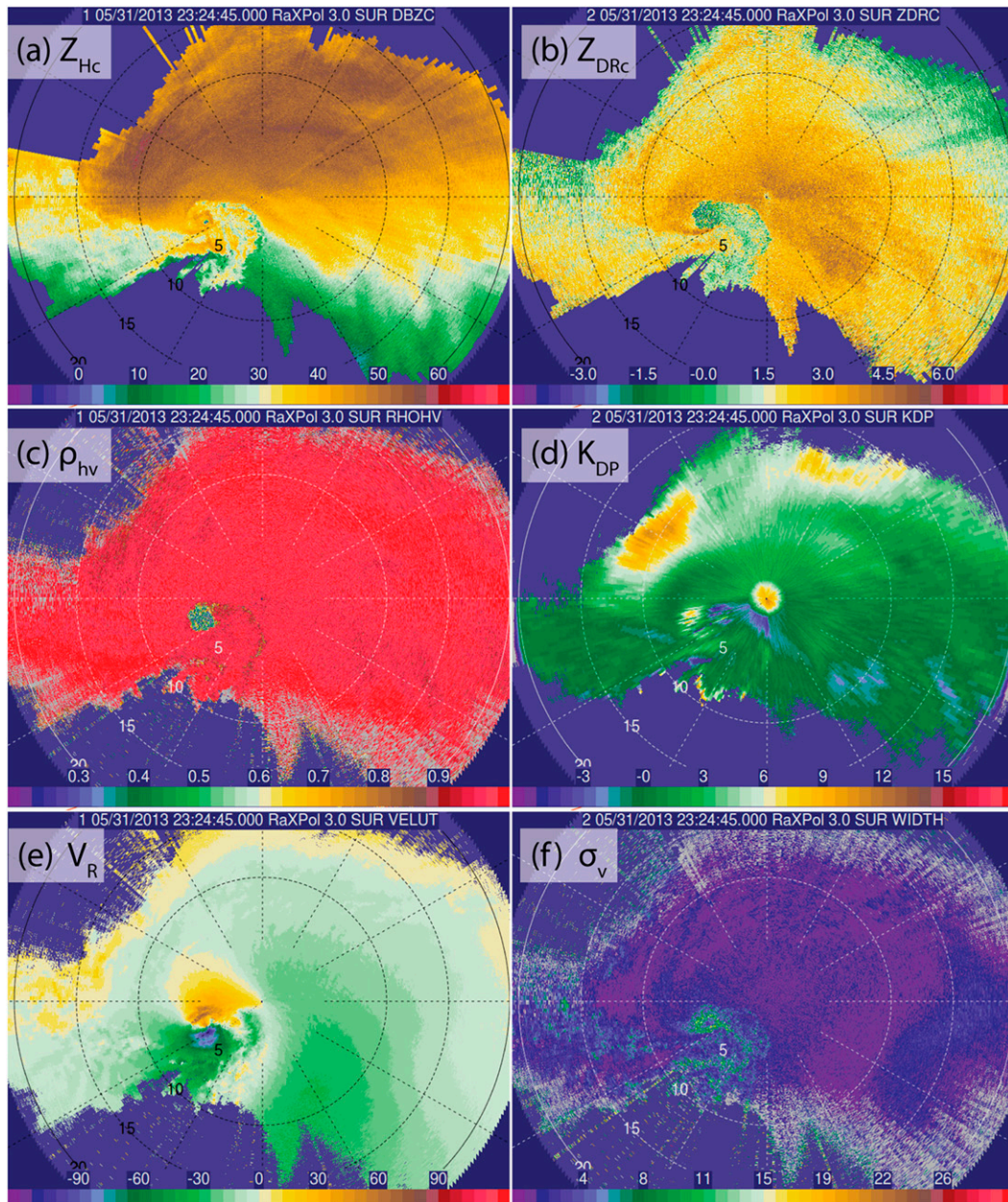
FIG. 7. (a) Attenuation-corrected Z_{Hc}, (b) attenuation-corrected Z_{DRc}, (c) ρ_{hv}, (d) K_{DP}, (e) V_R, and (f) σ_v valid at 2324:45 UTC 31 May 2013 showing the entirety of the supercell as sampled by RaXPol. Attenuation by rain has been approximately compensated for in (a),(b) by the use of the ZPHI method (Testud et al. 2000; Snyder et al. 2010) and a relation between attenuation and differential attenuation. Range rings are marked every 5 km.

2-s mean wind, assuming that V_R varies linearly with time between the two scans. For example, the 2-s average V_R from 0° scans at 2325:55 and 2325:57 UTC, times during which another intense subvortex was moving toward the radar, was ~109.3 m s^{-1} (Fig. 10), reduced from the 119.5 and 116.4 m s^{-1} V_R from the two individual scans. The boresight-aligned estimated theoretical beam height (not including ground elevation changes) was approximately −50 m AGL in Fig. 10, so only the very top extent of the "theoretical" beam was illuminated since part of the beam intercepted the ground and there was nearby ground clutter. There is an unknown contribution of scattering off the ground, and partial beam blockage from the ground and nearby clutter targets likely resulted in a very complex beam illumination pattern, making it impossible to know the
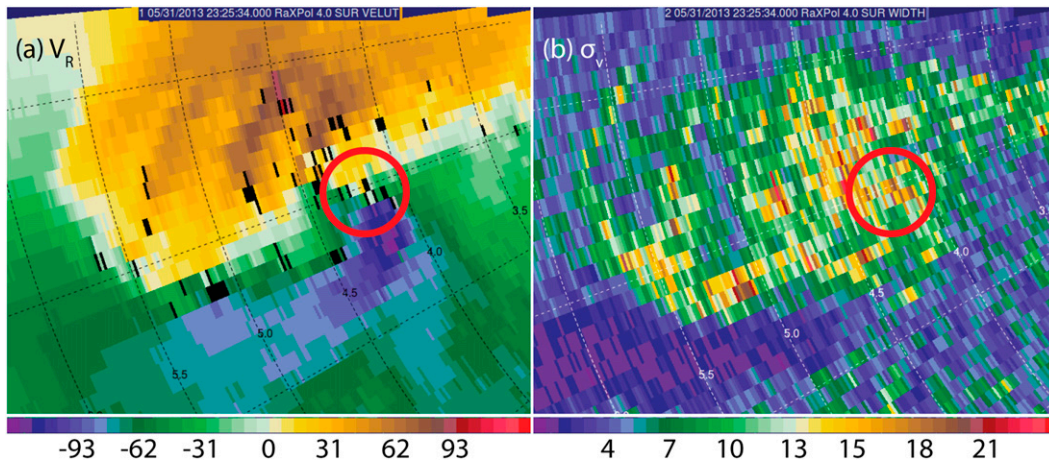
FIG. 8. Graphics of (a) V_R and (b) σ_v at 2325:34 UTC 31 May 2013 valid at 4°-elevation angle. An intense subvortex (marked by the red circle) is located in the southeastern section of the tornado. On the 0° (2325:25 UTC), 1° (2325:27UTC), 2° (2325:29 UTC), 3° (2325:32 UTC), and 4° (2325:34 UTC) sweeps from which this scan was taken, the peak V_R values within this subvortex are 130.4, 126.45, 130.4, 129.7, and 126.5 m s^{-1}, respectively.

distribution of scatterers that most significantly affected V_R. Regardless, it seems likely that the radar was sampling scatterers near the ground.

One of the most difficult aspects of rating this particular tornado (e.g., R. Smith 2013, personal communication) is that the extreme winds sampled by RaXPol [and a DOW (Wurman et al. 2014)] occurred over rural areas that had very few DIs present. For example, V_R of at least 135 m s^{-1} measured by RaXPol during D3 occurred over an open field that was devoid of substantial structures (Figs. 11b,c). Visits to this area showed that the extent of damage largely was limited to flattened vegetation and fences with perhaps some gravel scouring, although other structures were affected by weaker winds. There was an example of helical-shaped swaths of completely matted vegetation observed very near the location of one of the subvortices (Fig. 11c).

More detailed analyses of the evolution of the supercell and tornado are forthcoming. We note, however, that the hook echo and much of the eastern part of the tornado were characterized by anomalously low Z_{DR} given the relatively high Z_H and K_{DP} observed (e.g., Figs. 4 and 7). These characteristics suggest that the mean drop size was relatively small for the amount of rainwater in these areas, which is in agreement with a couple of studies that have examined Z_{DR} in the hook echoes of several tornadic supercells (e.g., Kumjian 2011; French et al. 2013).

There is an additional noteworthy observation in Φ_{DP}: in data collected at D3, there is a relatively small area (~300 m × 1000 m) of locally reduced Φ_{DP} (e.g., ~20°–25° reduction; Fig. 12) adjacent to the southeast periphery of the debris field; it appears that this marks

an area of significant negative backscatter differential phase δ. This area is characterized by Z_{DR} of approximately 1.5 dB, $\rho_{hv} > 0.95$, and $\sigma_v < 3$ m s^{-1}, and it persists throughout the deployment (not shown). The high ρ_{hv} indicates that the scatterers in this area are likely meteorological in origin. Scattering simulations at X band (not shown) indicate that $\delta > 0°$ in rain; $\delta < 0°$ can occur in hail. Although nonuniform beam filling (NBF) may not be negligible along the edge of the debris field in regions of high Z_H and Φ_{DP} gradients (Ryzhkov 2007), the NBF-produced biases tend to continue down the radial, which is not observed here.

b. 24 May 2011

RaXPol sampled a violent tornado at a range as close as 2 km near El Reno on 24 May 2011 (Houser 2013). When the tornado was rapidly intensifying near its closest approach to RaXPol, the radar was scanning only one elevation angle, providing 2-s updates at 1°-elevation angle. The range resolution was 75 m (oversampled every 15 m), and 12 pulse pairs (i.e., 24 pulses) were used to calculate the moments. The highest V_R within this tornado measured by RaXPol occurred near 2100:39 UTC (~132.1 m s^{-1}; Fig. 13a). At this range (4 km) and elevation angle, the boresight-aligned theoretical beam height, after accounting for platform pitch and roll, was ~22 m ARL.

Two consecutive scans from 2100:39 and 2100:41 UTC have been averaged to yield an estimated 2-s mean V_R of 118.4 m s^{-1} (Fig. 13b). An average of three consecutive scans between 2100:39 and 2100:43 UTC yields an estimated 4-s average V_R of 110.8 m s^{-1} (Fig. 13c). Note that this is only averaging one component of the flow in the tornado (the radar-directed radial component), so it
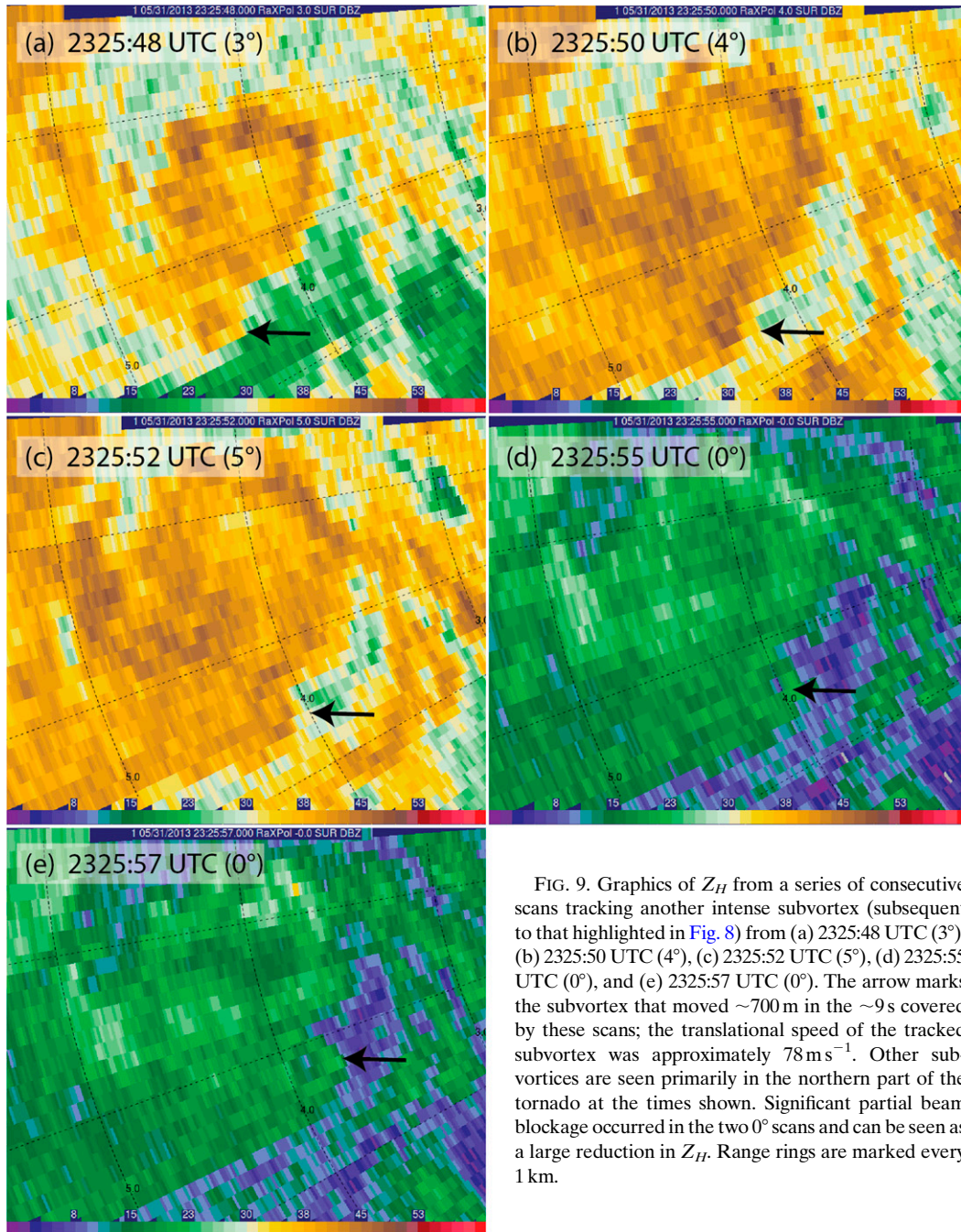
FIG. 9. Graphics of Z_H from a series of consecutive scans tracking another intense subvortex (subsequent to that highlighted in Fig. 8) from (a) 2325:48 UTC (3°), (b) 2325:50 UTC (4°), (c) 2325:52 UTC (5°), (d) 2325:55 UTC (0°), and (e) 2325:57 UTC (0°). The arrow marks the subvortex that moved ~700 m in the ~9 s covered by these scans; the translational speed of the tracked subvortex was approximately 78 m s^{-1}. Other subvortices are seen primarily in the northern part of the tornado at the times shown. Significant partial beam blockage occurred in the two 0° scans and can be seen as a large reduction in Z_H. Range rings are marked every 1 km.

is likely to be an underestimate of the true 2- and 4-s-average wind speeds.

4. On the accuracy of V_R estimates in tornadoes

a. Velocity estimate errors

There are statistical errors in V_R estimates because there are only a limited number of samples from which to calculate V_R. When PPP (as it has been with RaXPol) is used, V_R is calculated as

$$V_R = -\frac{\lambda}{4\pi T_s} \arg[\hat{R}(T_s)], \tag{1}$$

where λ is the radar wavelength, T_s is the pulse repetition time, arg represent the argument of the complex quantity, and $\hat{R}(T_s)$ is the autocorrelation function
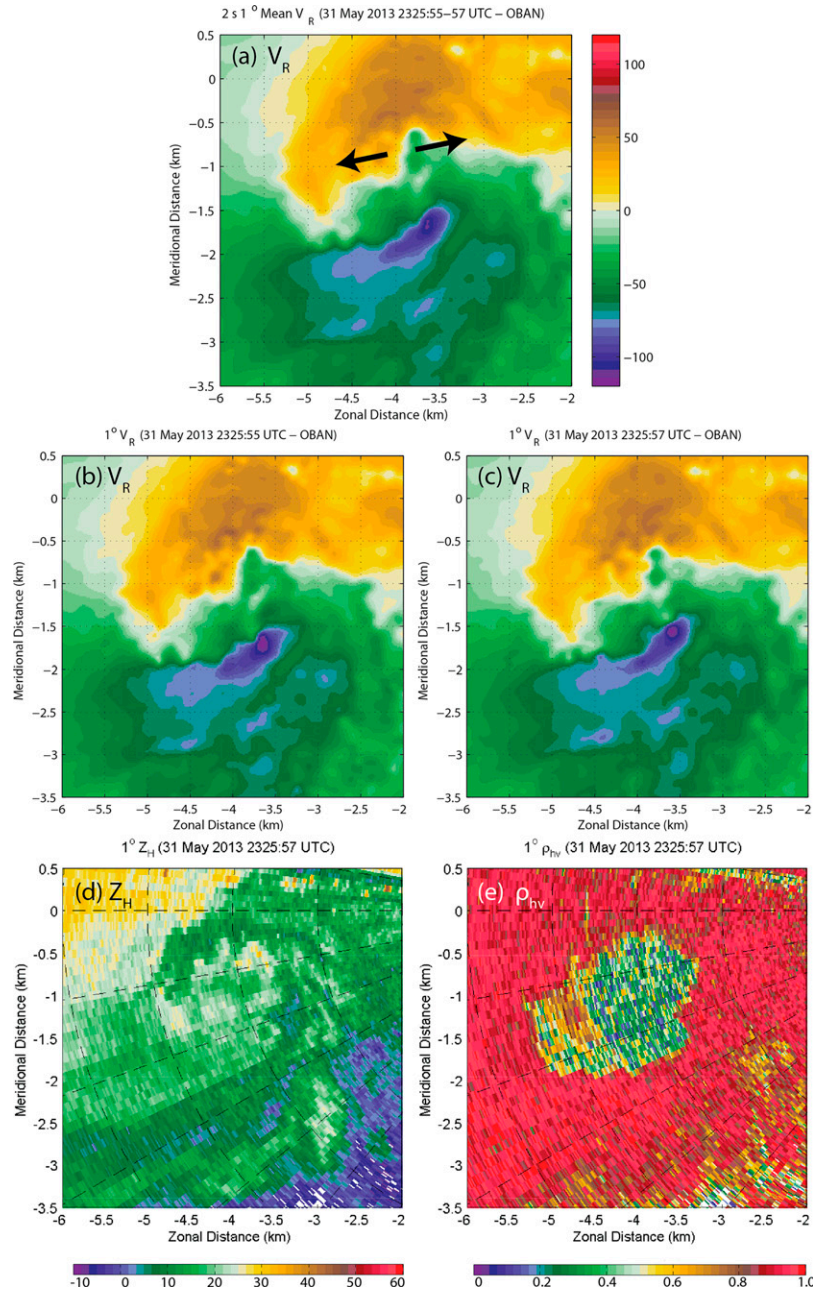
FIG. 10. RaXPol data from 2325:55 to 2325:57 UTC 31 May 2013 valid at a truck-relative elevation angle of 0.0° objectively analyzed using a two-pass Barnes scheme with horizontal grid spacing of 15 m, $\kappa = 0.0097\,\mathrm{km}^2$, and $\gamma = 0.3$: (a) an average V_R using two consecutive scans separated by 2 s, (b) analyzed V_R at 2325:55 UTC, (c) analyzed V_R at 2325:57 UTC, (d) Z_H, and (e) ρ_{hv}. In (a)–(c), gates with NCP < 0.2 have been removed, and the analysis linearly interpolated V_R for such gates. Accounting for nonzero platform pitch and roll, the antenna boresight-aligned estimated beam height through the tornado center is approximately −50 m ARL; partial beam blockage from nearby trees and other structures, as well as significant ground interception as an increasing amount of the radar beam hit the ground, essentially left only the top part of the antenna pattern illuminated. Range rings are plotted every 1 km. The maximum inbound averaged V_R in (a) is 109.3 m s^{-1}; the maximum V_R in (b) and (c) is 119.5 and 116.4 m s^{-1}, respectively. Strong radial divergence is observed near the center of the tornado [denoted by black arrows in (a)], potentially indicating that the tornado has primarily a two-cell structure. Axes labels are relative to the radar location.
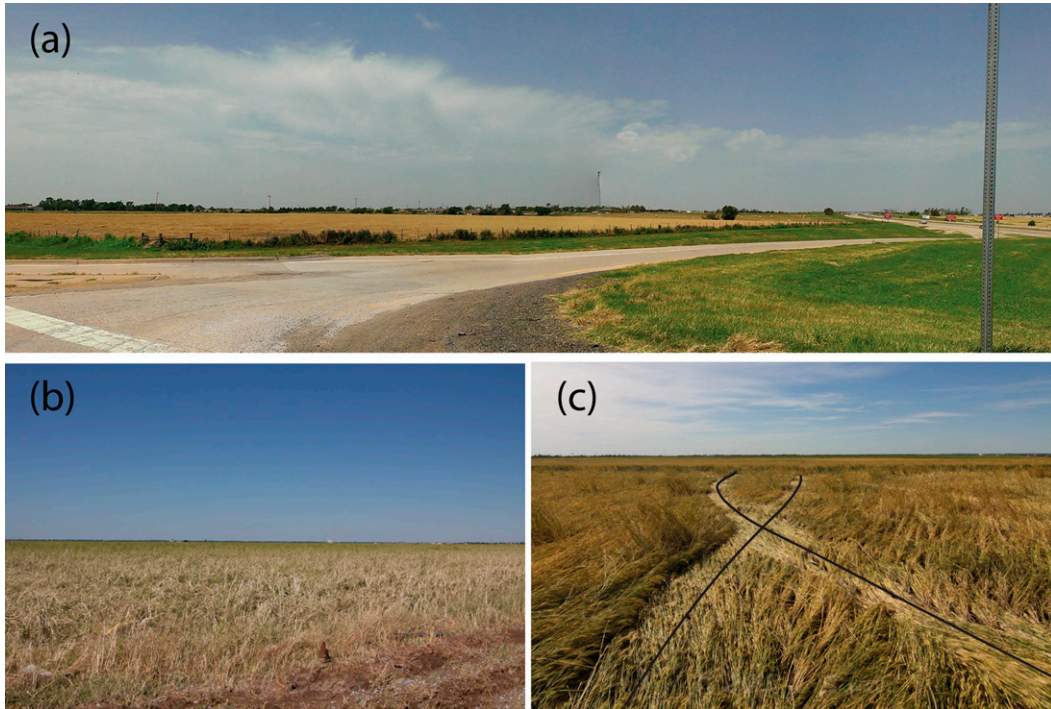
FIG. 11. (a) A panoramic photograph from very near the third deployment location (D3, marked by a yellow pushpin along the right side of Fig. 2a) on 31 May 2013 taken several weeks after the tornado. View is to the west-northwest on the right side of the photo and to the south-southwest on the left side of the photo. Interstate 40 (I40) is visible on the right side of the photo; the photo was taken just off the eastbound exit from I40 on Banner Road. (b) A photograph taken from near the green star in Fig. 2a looking to the northeast, where the strongest winds were measured by RaXPol. (c) A photograph (view to the northwest) from the location represented by the orange star in Fig. 2a. Note the helical damage swaths, marked by black curves in (c), in which the thick foliage was matted to the ground; each "swath" was ≤1 m wide. [Photograph courtesy of J. Snyder.]

at lag 1. If the transmit frequency is changed by at least the inverse of the pulse bandwidth from pulse group to pulse group (i.e., pulse pairs are independent, or at least relatively uncorrelated), $\hat{R}(T_s)$ can be calculated as

$$\hat{R}(T_s) = \frac{1}{M} \sum_{m=0}^{M-1} V(2m+1)V(2m), \qquad (2)$$

where M is the number of independent pulse pairs.

According to Zrnić (1977), the variance of the mean estimate (V_R) determined by PPP can be calculated as shown in Eq. (6.21) in DZ93. The variance of V_R can be estimated as [see Eq. (6.22b) in DZ93]

$$\text{var}(\hat{V}_R) \approx \lambda^2 \frac{\left(1 + \frac{N}{S}\right)^2 - \rho^2(T_s)}{32\pi^2 M \rho^2(T_s) T_s^2}, \qquad (3)$$

where

$$\rho(T_s) = \exp\left[-8\left(\frac{\pi\sigma_v T_s}{\lambda}\right)^2\right] = \exp\left[-\frac{(\pi\sigma_{vn})^2}{2}\right] \quad (4a)$$

and σ_{vn} is the normalized spectrum width defined as in Melnikov (2004):

$$\sigma_{vn} = \frac{\sigma_v}{V_a} \qquad (4b)$$

and

$$V_a = \frac{\lambda}{4T_S}. \qquad (4c)$$

Consider a high-V_R observation $(135.0 \, \text{m s}^{-1})$ from 31 May 2013 near 2325 UTC. For a typical "worst case" scenario, $\sigma_v = 15 \, \text{m s}^{-1}$ with $M = 8$, $T_s = 0.25 \times 10^{-3} \, \text{s}$, and SNR $\sim$30 dB yields V_R variance (3) of $\sim$56.5 m^2 s^{-2} or a standard deviation of $\sim$7.5 m s^{-1}. So, the estimated V_R is $135.0 \pm 7.5 \, \text{m s}^{-1}$ when describing ± 1 standard deviation about the mean estimate. In most of the RaXPol observations of intense tornadoes at close
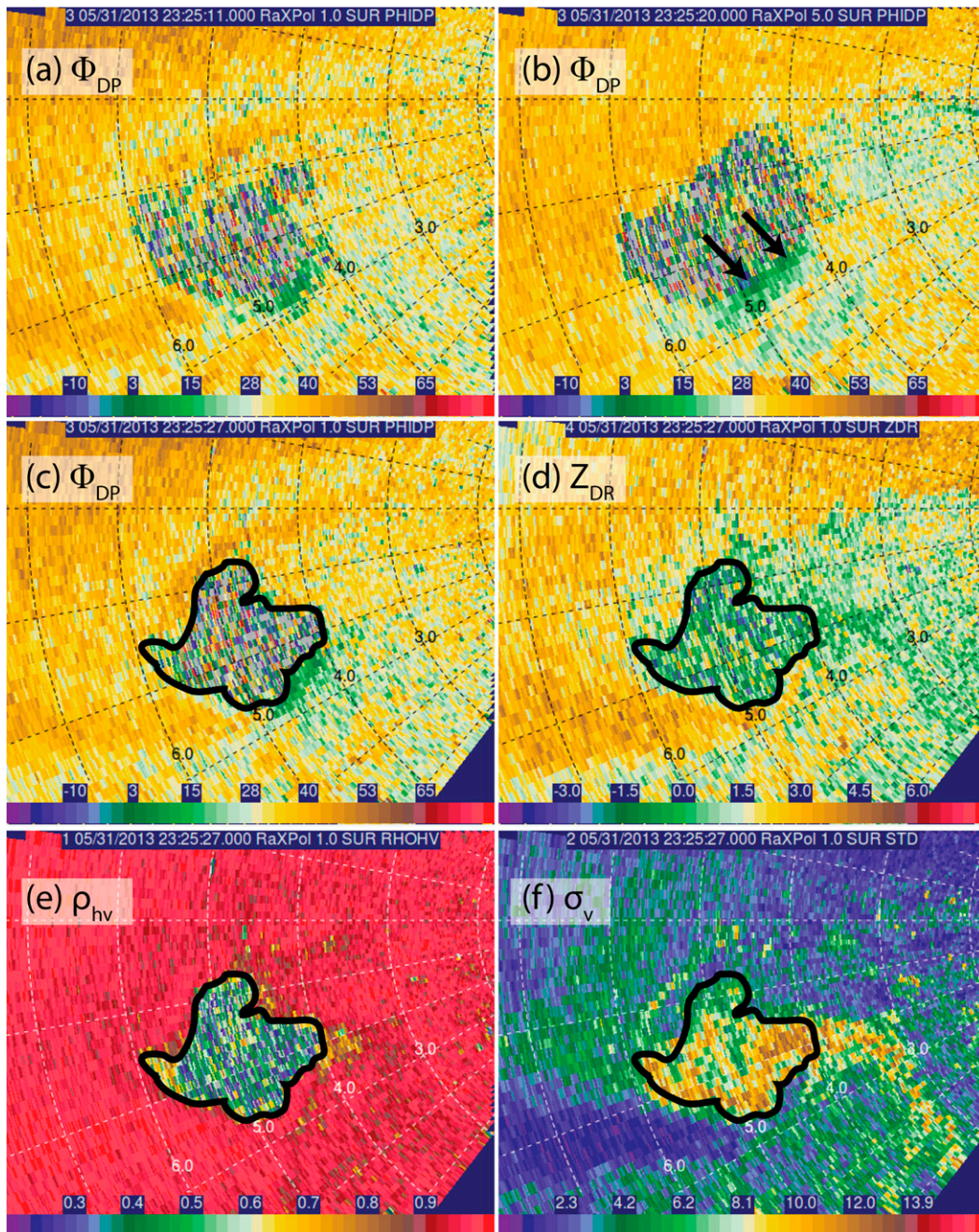
FIG. 12. An area of anomalously low Φ_{DP}, marked by black arrows in (b), in the southeast part of the tornado during the third deployment as observed at (a) 2325:11 UTC (1°-elevation angle), (b) 2325:20 UTC (5°-elevation angle), and (c) 2325:27 UTC (1°-elevation angle). Values of Φ_{DP} in this area are ~20°–25° lower than the "background" Φ_{DP} along the affected radials. Given the local nature of the reduction, this area, which persists for nearly the entire deployment, seemingly marks a region of scatterers with backscatter differential phase considerably less than 0°. Collocated with the reduced Φ_{DP} are (d) Z_{DR} of ~2 dB, (e) $\rho_{hv} > 0.95$, and (f) $\sigma_v < 3 \, \mathrm{m \, s^{-1}}$ (from 2325:27 UTC). The black enclosed shape in (c)–(f) is the approximate edge of the tornadic debris field (e.g., $\rho_{hv} < 0.8$).

range, SNR is typically quite high (i.e., >30 dB), so further discussion will generally assume high SNR. One could expand the V_R "bounds" by including σ_v, but one would then generally want to take the high end of this

range if one is interested in the maximum speed within the resolution volume.

Note that (3) and (4a) assume that the Doppler spectrum has a Gaussian distribution, which is a dubious
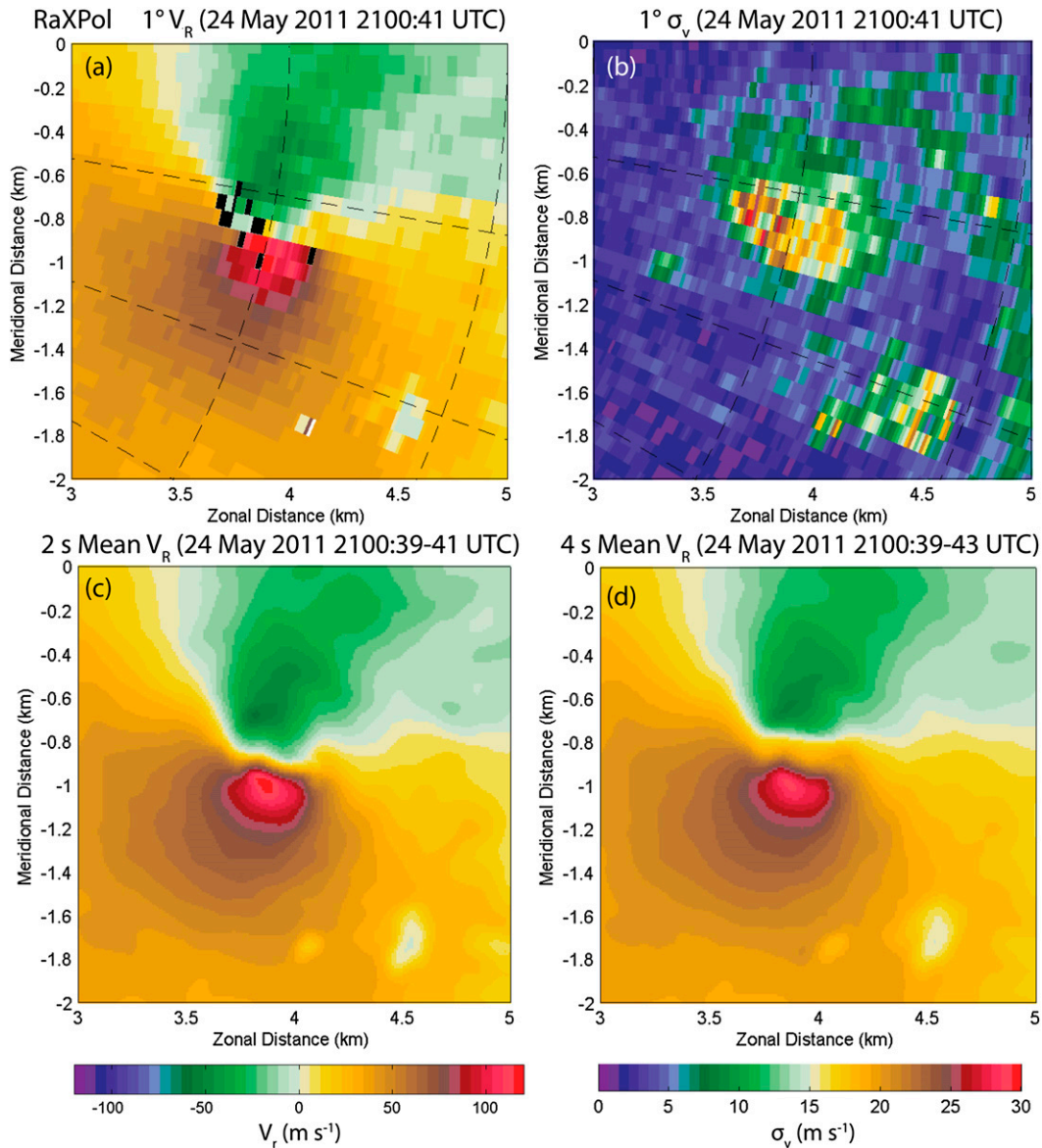
FIG. 13. (a) Measured V_R and (b) σ_v at 2100:41 UTC 24 May 2011 southeast of El Reno. Two-pass Barnes analyses (15-m grid spacing, $\kappa = 0.0097\,\mathrm{km}^2$, and $\gamma = 0.3$), for three sweeps collected at 2100:39, 2100:41, and 2100:43 UTC were created, from which the (c) 2-s-mean V_R between 2100:39 and 2100:41 UTC and the (d) 4-s-mean V_R using all three scans were created. All data were collected at a 1.0° radar-relative elevation angle (refer to Fig. 17b for estimated beam height accounting for pitch and roll). The maximum V_R in (a) is 132.1 m s^{-1}; the maximum objectively analyzed V_R at the same time is 129.4 m s^{-1}. The maximum 2-s- and 4-s-mean V_R values are 118.4 and 110.8 m s^{-1}, respectively. Range rings are plotted every 1 km in (a),(b). Black gates in (a) are removed owing to having NCP < 0.2.

assumption for radar volumes in a debris-filled tornado (e.g., Bluestein et al. 1993). It is very difficult to estimate the variance of V_R without knowing or assuming the shape of the spectrum, however, and, owing to the frequency hopping used by RaXPol in "rapid scan" mode, retrieving the Doppler spectra from RaXPol observations is currently not possible unless the scanning rate is slowed to more "traditional" speeds and frequency

hopping is disabled. By the nature of a distribution with nonzero width, the mean V_R of scatterers within a resolution volume (i.e., the V_R measured by radar) will be lower than the peak V_R of the fastest-moving scatterers. In (3) and (4), σ_v is assumed to be small compared to the maximum unambiguous velocity V_a. From Melnikov and Zrnić (2004), the calculated σ_v will be negatively biased when the true σ_v is larger than $\sim 0.6 V_a$.

b. The influence of debris and reduced ρ_{hv} on velocity estimates

From observations it is seen that σ_v within tornadoes can be large on account of the differential velocity of scatterers in regions of very strong accelerations and large gradients in flow characteristics. Enhanced σ_v increases the expected variance of the V_R estimate (e.g., Fig. 6.5 in DZ93). A radar volume filled with hydrometeors and debris of varying shapes and sizes will have a comparatively wide Doppler spectrum owing to the different velocities characterizing the scatterers. Since the expected variance of V_R is sensitive to σ_v (which, in many RaXPol tornado datasets, is enhanced within the PTDS), the presence of debris and high σ_v tends to increase the V_R variance.

The variance in V_R calculated by PPP is affected by the number of samples used to calculate the moments (i.e., M), particularly when the number of independent samples is relatively low [i.e., $O(10)$; note the M^{-1} dependence in (3)]. Typically, meteorological echoes are associated with relatively high ρ_{hv} (e.g., Straka et al. 2000; Park et al. 2009; Dolan and Rutledge 2009; Snyder et al. 2010), which, by definition, means that the H and V channels are highly correlated at lag time 0 and, thus, the combination of data from the two channels is unlikely to increase the quality of the mean V_R estimate compared to that from only one channel (assuming the SNR is not particularly low).

In the tornadic debris field, ρ_{hv} is markedly reduced (e.g., Ryzhkov et al. 2005; Kumjian and Ryzhkov 2008; Bluestein et al. 2007a; Snyder et al. 2010; Bodine et al. 2013). The signals from the H and V channels are therefore less correlated than in areas composed of purely meteorological scatterers. In areas of high ρ_{hv}, using M pulse pairs in H and V still yields approximately M independent pulse pairs; in areas of low ρ_{hv}, transmitting M pulse pairs in the H and V channels yields up to $2M$ pseudoindependent pulse pairs (for $\rho_{hv} \sim 0$). Polarimetric-based V_R estimates using H and V channels should have reduced variance within the debris field compared to V_R from a single channel (or single-polarization radar). Consider the expected variance of a V_R field defined as the average of V_H and V_V:

$$V_R = \frac{V_H + V_V}{2}. \tag{5}$$

The variance of (5) is

$$\text{var}\left(\frac{V_H + V_V}{2}\right) = \frac{\text{var}(V_H) + \text{var}(V_V) + 2\,\text{cov}(V_H, V_V)}{4}. \tag{6}$$

The ratio of the variances of the "polarimetric" V_R to the estimate obtained using only the H channel (i.e., V_H), assuming the noise levels in each channel are the same and $Z_{DR} \approx 0\,\text{dB}$, is shown in Melnikov [(2004); Eq. (6.3)] as

$$\frac{\text{var}(V_R)}{\text{var}(V_H)}$$
$$= \frac{1}{2}\left\{1 + \rho_{hv}^2\left[1 + \frac{\{2\text{SNR}[1 - \rho(T_s)^2] + 1\}M_1}{\{1 - \rho(T_s)^2\}(M - 1)\text{SNR}^2}\right]^{-1}\right\}, \tag{7}$$

where M_1 is the number of independent samples in $M - 1$ samples. When ρ_{hv} or SNR is low, this ratio is less than 1, indicating a reduction in the variance of the "polarimetric" V_R relative to that in the single-polarization V_H estimate (Fig. 14); when ρ_{hv} and SNR are high, there is little reduction in the variance of V_R relative to that of V_H. Note that σ_v affects (7) through its effect on $\rho(T_s)$ in (4a); all else being equal, an increase in σ_v at a given T_s (i.e., an increase in σ_{vn}) generally increases (7), although this effect is really only evident at low SNR (e.g., SNR < 10 dB). As it relates to the PTDS, even at high SNR, (7) can be significantly affected by ρ_{hv}. Particularly where $\rho_{hv} < 0.7$, (7) will be less than unity, signaling that the addition of data from the second, orthogonally polarized channel reduces the expected variance of V_R.

As an alternative to (5), a polarimetric V_R estimate can be obtained by averaging the lag 1 autocovariances from each channel before calculating V_R:

$$\hat{R}(T_s) = \frac{\hat{R}_h(T_s) + \hat{R}_v(T_s)}{2}. \tag{8}$$

In calculating V_R using PPP, we are interested in the argument of $\hat{R}(T_s)$, and the variance of V_R calculated using (8) and (1) and its ratio to the variance of a single-polarization V_H is considerably more complex than that shown in (7) [see Eq. (6.5) in Melnikov (2004)]. However, the reduction in the variance of V_R using (8) is very similar to that obtained using (5) (Melnikov 2004). The RaXPol V_R observations presented in this paper have been calculated according to (8).

c. Differential velocity

Although Z_{DR} has received considerable attention in the literature following Seliga and Bringi (1976), radar-estimated differential radial velocity V_D in tornadoes has not been formally examined. As previously noted, where ρ_{hv} is ~1 (i.e., for meteorological scatterers), V_R estimates from the H (V_H) and V (V_V) channels should be very similar. However, where nonmeteorological
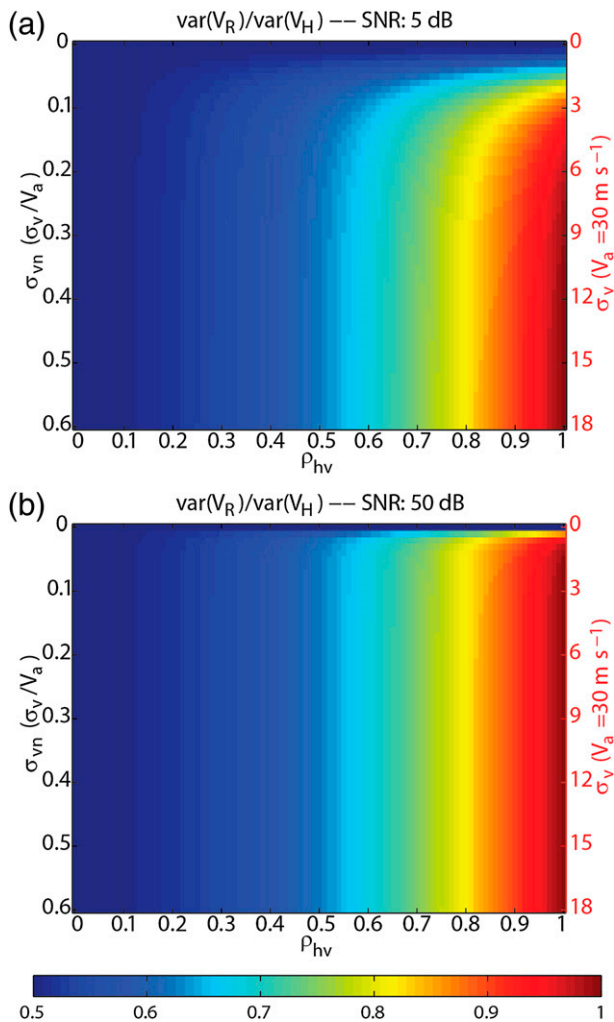
FIG. 14. The ratio of the variance of the polarimetric V_R estimate to the variance of the single-polarization V_H estimate using 11 pulse pairs at (a) 5- and (b) 50-dB SNR. The value of ρ_{hv} increases to the right along the abscissa; σ_{vn} increases downward along the left ordinate. The equivalent σ_v for $V_a = 30\,\mathrm{m\,s^{-1}}$ (similar to what it was during D2 and D3 on 31 May 2013) is shown on the right ordinate in red. Ratios less than 1.0 indicate a decrease in the variance of the velocity estimate when H and V channel data are included relative to when only the H channel is used.

scatterers are abundant (e.g., tornado debris), appreciable reduction in ρ_{hv} and very complex scattering behavior may result in significantly different V_H and V_V. Differential velocity is herein defined simply as

$$V_D = V_H - V_V. \qquad (9)$$

Since V_R is a reflectivity-weighted mean estimate, a volume composed of scatterers with large aspect ratios, nonzero mean canting angles, and a wide range of V_R can yield much different Doppler spectra in the H channel from those in the V channel. For example, the

magnitude of V_D may exceed more than a few meters per second when biological scatterers are present (Melnikov et al. 2014). In examining RaXPol observations, we have identified large V_D within the PTDS. For example, in the PTDS from 2325 UTC on 31 May 2013, the magnitude of V_D exceeds $10\,\mathrm{m\,s^{-1}}$ (Fig. 15). It is seen, upon calculating the mean and standard deviations of V_D as a function of ρ_{hv} (Fig. 16), that, at least in the 2325:55 and 2325:57 UTC 0° scans used to compute these statistics, the mean V_D deviates very little from $0\,\mathrm{m\,s^{-1}}$, and the standard deviation of V_D increases with decreasing ρ_{hv}.

From examples of V_D from scans collected at close range (3–4 km) and low-elevation angles within violent tornadoes sampled by RaXPol on 24 May 2011 near El Reno (Fig. 17), and on 19 May 2013 near Shawnee, Oklahoma (Fig. 18), we find that V_D of $O(10)\,\mathrm{m\,s^{-1}}$ is associated with regions of low ρ_{hv} and high σ_v; V_D differs from $0\,\mathrm{m\,s^{-1}}$ most significantly where low ρ_{hv} is juxtaposed with high σ_v. A similar observation is noted with an earlier tornado that occurred northeast of Oklahoma City on 19 May 2013 (Fig. 19). As a result, V_D may be an additional parameter useful for detecting tornadic debris from ongoing tornadoes. Given that areas where the magnitude of V_D exceeds a few meters per second also tend to have enhanced σ_v, some of the deviation of V_D from $0\,\mathrm{m\,s^{-1}}$ is attributable to statistical limitations of estimating V_R given a limited number of samples. In this way, V_D may be a proxy for σ_v, although V_D does not follow σ_v as well outside the debris signature (or at least outside areas with low ρ_{hv}); high V_D in RaXPol datasets occurs when *both* parameters are favorable (such as is typically the case in high-resolution radar observations of tornadoes). Since time series data are not available for the RaXPol datasets examined in this study, analyses of spectral differential reflectivity (Melnikov et al. 2014) and more detailed examination of the Doppler spectra in each channel are not possible. It is possible that analyses of V_D within tornado debris signatures may reveal some information about debris characteristics.

5. Summary

As the number of mobile radar datasets of tornadoes increases, the complicated question of how such data may be used when estimating tornado intensity inevitably arises. The EF scale, and the original F scale before it, arguably are intended to aid in the determination of the intensity of winds within tornadoes (under the constraint of a 3-s-average wind speed measured at 10 m AGL) by using tornado damage as a proxy. Determining DoDs in a tornado can be quite difficult, and the wind speed ranges expected for some DoDs and
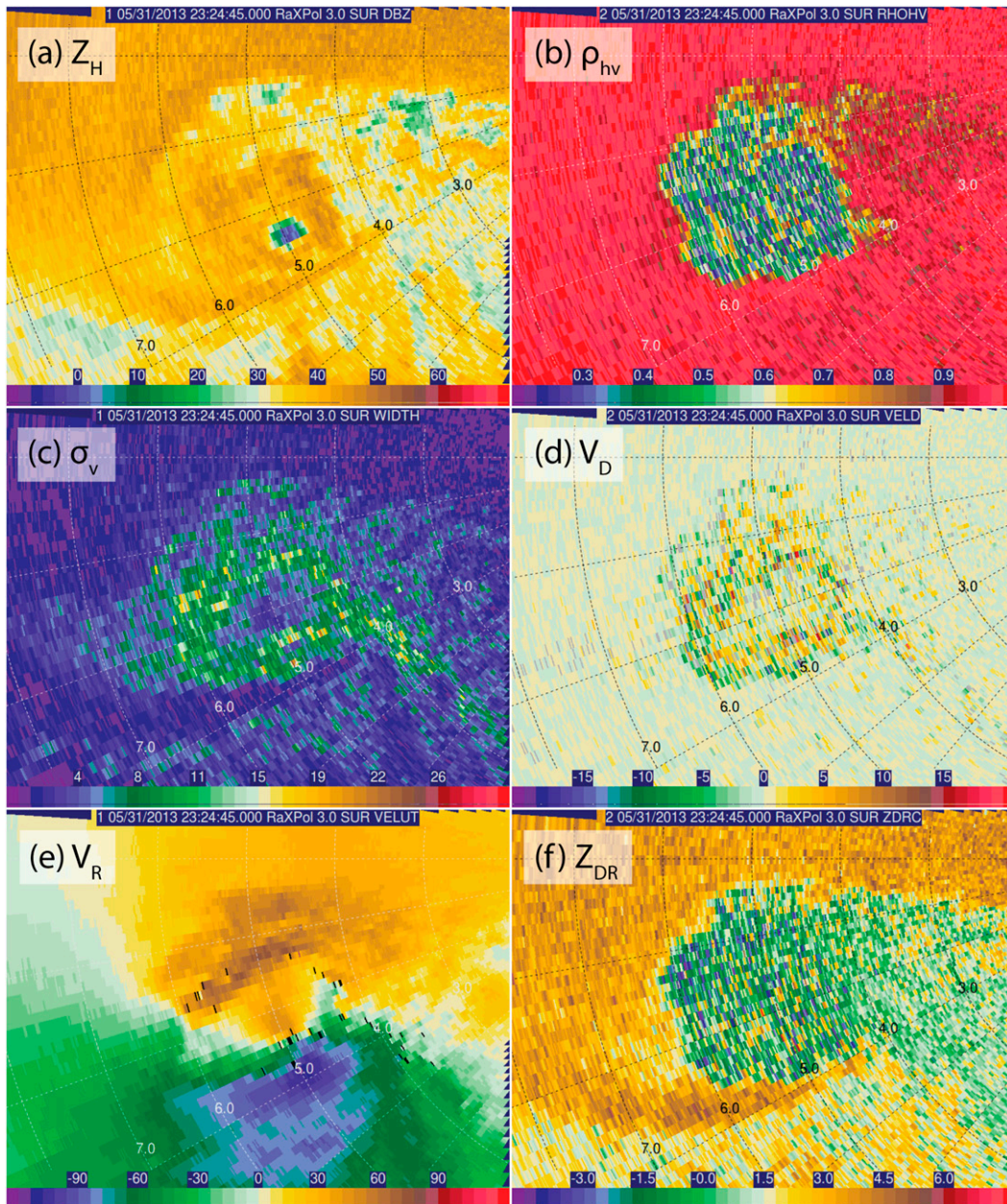
FIG. 15. Graphics of RaXPol (a) Z_H, (b) ρ_{hv}, (c) σ_v, (d) V_D, (e) V_R, and (f) Z_{DR} at 2345:45 UTC 31 May 2013 at a radar-relative elevation angle of 3.0°. Range rings are marked every 1 km, with spokes provided every 10° in azimuth.

DIs can span several EF-scale categories. As such, one can argue that actual high-resolution measurements of winds can aid in the assessment process, particularly when damage exceeds the maximum DoD for affected DIs. Although commentary on the use of radar data in the EF-scale rating process as used by official entities or organizations is beyond the scope of this paper, it does seem prudent, in some as-yet-undetermined manner, to consider all available observations (whether they be in situ anemometer observations or remote sensing data available by radar), especially when damage assessment is particularly difficult and assuming the ultimate use of the EF scale is to determine tornado intensity. There is likely to be value in including additional observations if such observations are used in a clear, consistent, and careful manner, even if such observations are unable to be used as the sole basis for an EF-scale rating. The authors suggest, as one possibility, the addition of a plus
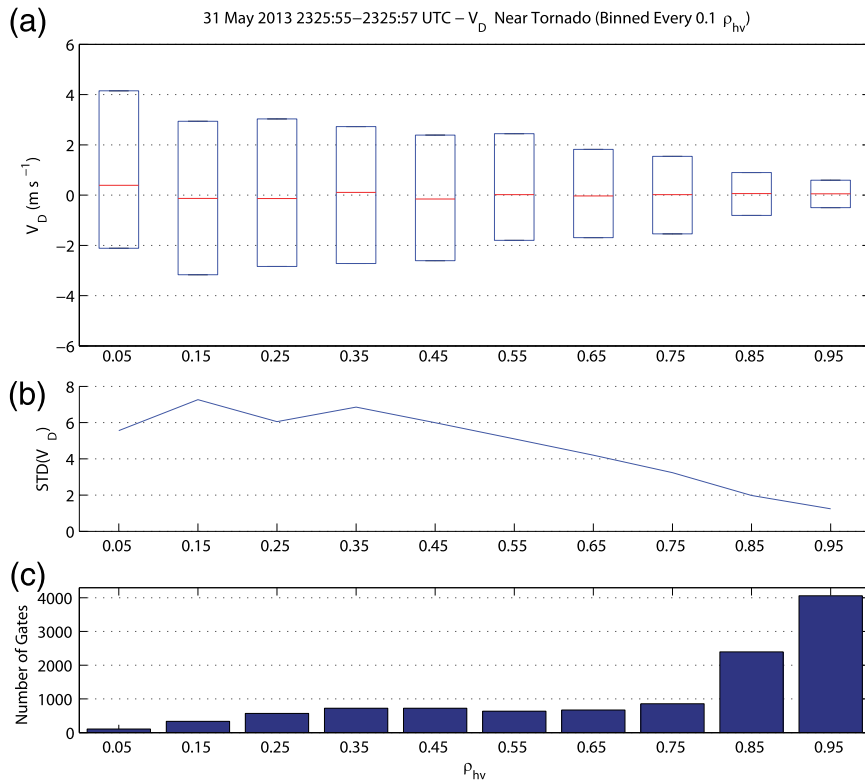
(a)
$$31 \text{ May } 2013 \text{ } 2325{:}55{-}2325{:}57 \text{ UTC} - V_D \text{ Near Tornado (Binned Every } 0.1 \text{ } \rho_{hv})$$

FIG. 16. Differential velocity (V_D; m s^{-1}) from the 2325:55 and 2325:57 UTC scans at 0°-elevation angle are binned according to the ρ_{hv} value within each gate near and within the tornado debris signature. (a). A box plot of V_D in 0.1-ρ_{hv} bins with the top and bottom of each box representing the 75th and 25th percentiles respectively, and the red line representing the mean value of V_D for all gates within each ρ_{hv} bin. (b) A plot of the standard deviation of V_D within each ρ_{hv} bin. (c) The number of gates within each bin.

(i.e., "+") modifier to EF-scale ratings assigned by entities that wish to continue to rate tornadoes based solely on damage, whereby, if so desired, an EF-scale rating may be assigned based exclusively upon damage, but an additional plus modifier can be added if there is compelling evidence from other sources that wind speeds likely exceeded those associated with the damage-determined EF-scale rating. For example, the El Reno tornado observed on 31 May 2013 has been rated an EF3 (as of February 2014 per *Storm Data*) based upon damage, whereas the authors support a rating of "EF3+" to denote that the EF3 rating is a lower bound and that there are credible, high quality, non-damage-based observations indicating wind speeds significantly greater than those associated with the EF3 rating.

It is important to keep in mind what V_R measurements contained in a radar dataset actually provide; they are estimates of the radar-relative radial component of the reflectivity-weighted, ensemble-averaged velocity of all scatterers within (neglecting sidelobe contamination) a nondiscrete radar volume collected during a dwell time that is orders of magnitude shorter than the 3-s

EF-scale criterion. Most of the characteristics of V_R tend to contribute to V_R underestimating the EF-scale-equivalent winds, while a few factors (primarily the relationship between a nearly instantaneous V_R observation and the 3-s-average wind speed) tend to contribute to V_R overestimating the EF-scale-equivalent winds. Perhaps the most significant uncertainty when applying V_R observations to EF-scale-equivalent winds is how the V_R for a given resolution volume relates to the 10 m AGL height criterion of the EF scale. Unfortunately, there are only very limited observations of the vertical profile of winds within the lowest 20–50 m of tornadoes owing to the extreme difficulty in safely obtaining such measurements. In most observations, it seems that there is no clear, consistent relationship between the observed V_R at or above 50 m AGL, for example, and the winds that occur at 10 m AGL; some observations (e.g., Kosiba and Wurman 2013) show the highest V_R occurring below 10 m AGL, generally corroborating published numerical simulations and theory.

RaXPol observed three violent tornadoes in central Oklahoma in 2011 and 2013 from less than 4-km range.
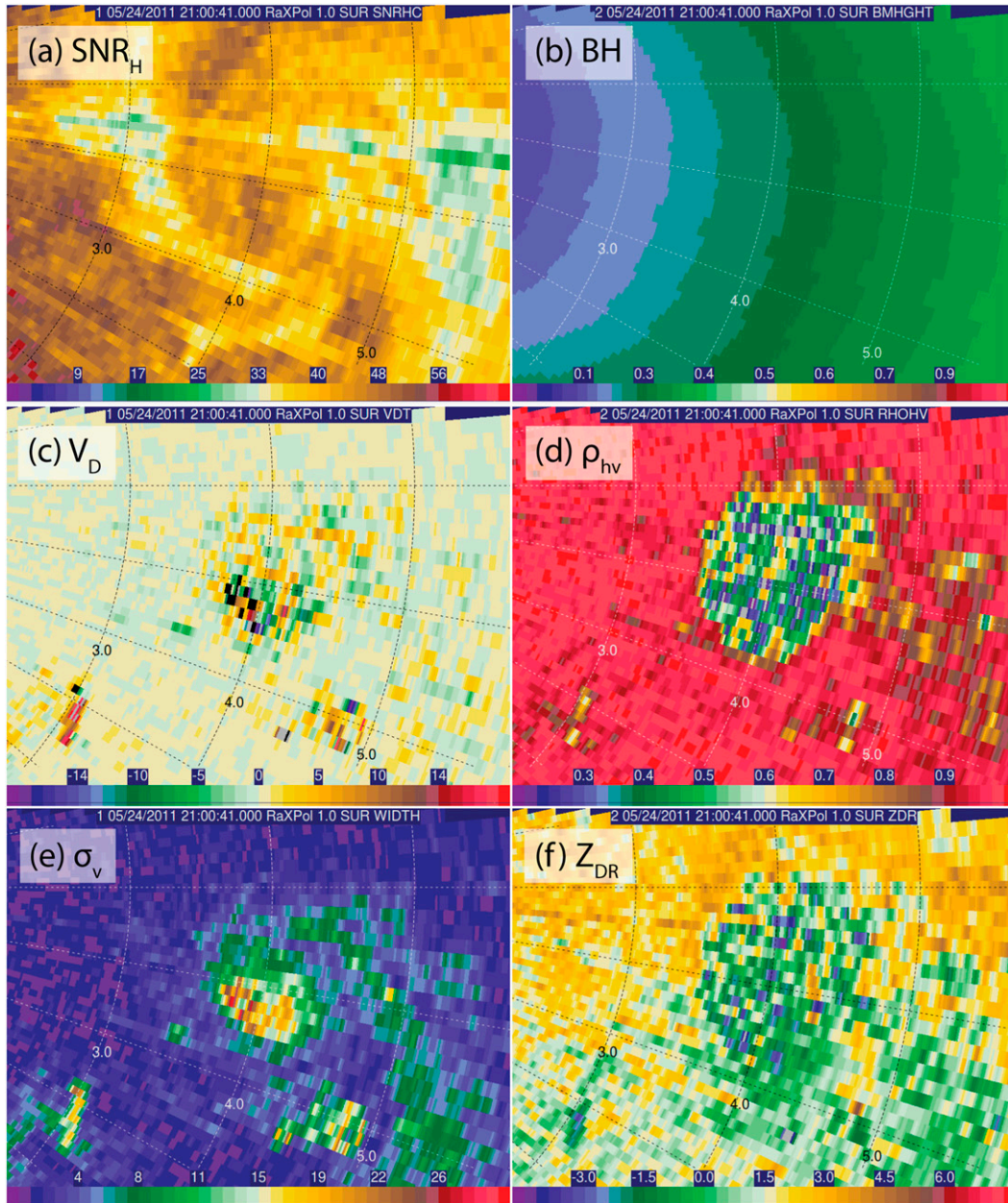
FIG. 17. Data from an intense tornado southwest of El Reno on 24 May 2011 valid at 2100:41 UTC at a range of ~4 km east-southeast of RaXPol: (a) SNR at H polarization, (b) estimated beam height above radar level (including pitch and roll; units are 10^2 m), (c) V_D, (d) ρ_{hv}, (e) σ_v, and (f) Z_{DR}. Range rings are marked every 1.0 km, and spokes are shown every 10° in azimuth. The V_R from this scan can be seen in Fig. 13.

Having the ability to collect a 360° sweep every 2 s allows us to estimate the 2-s-average V_R. On 31 May 2013, at the time examined (2325:55–2325:57 UTC), the 2-s-average V_R was approximately 5%–10% lower than the peak nearly instantaneous V_R. On 24 May 2011, the 2-s-average V_R was ~20% lower than the nearly instantaneous peak V_R. How well a 2-s-average V_R compares to the true 3-s-mean wind at a given point is likely to be highly dependent upon the forward motion of the tornadic wind field and any perturbations (e.g., subvortices) moving through/within it. In the case of multivortex tornadoes with extremely rapidly translating subvortices, the highest V_R may only occur over a particular area for a very short period of time. The effect of this fast movement, however, on the damage sustained by structures near the ground is unknown.
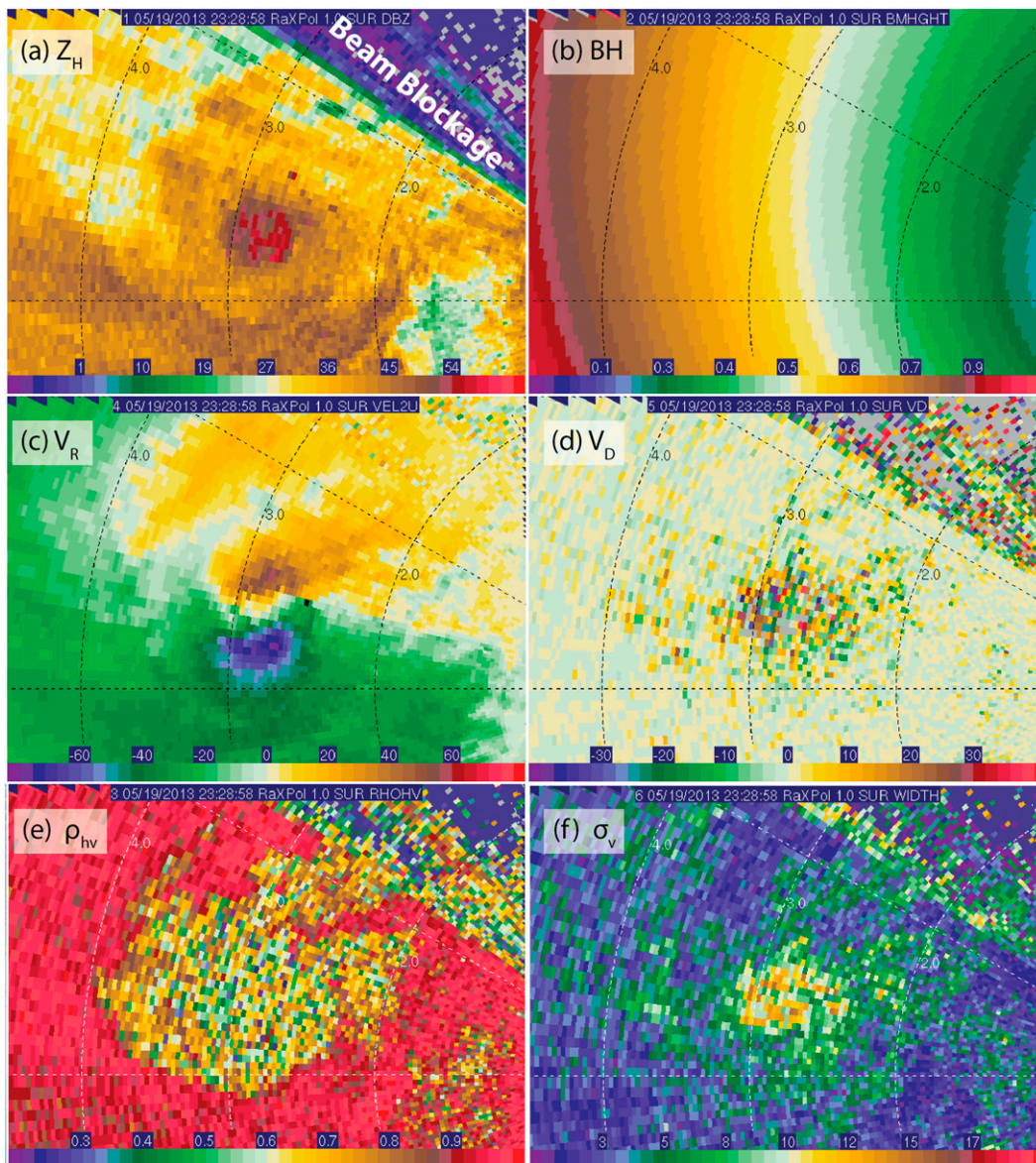
FIG. 18. RaXPol data valid at 2328:58 UTC 19 May 2013, capturing a strong tornado near Shawnee: (a) Z_H, (b) estimated beam height above radar level (units of 10^2 m), (c) V_R, (d) V_D, (e) ρ_{hv}, and (f) σ_v. Maximum V_R at this time is 80.5 m s^{-1} at a boresight-aligned height of approximately 52 m ARL. The scanning strategy differed from that during the data collected on 31 May 2013; here, volumetric data were collected at elevation angles of 1°–19° every 2° (yielding volume update times of ~32 s) using staggered PRT. Note that the V_R shown in (c) is manually unfolded from the V_R calculated from the pulse pair with the lowest PRT; V_D is produced from V_H and V_V calculated from the staggered PRT method. Range rings are plotted every 1 km.

As it pertains to tornadoes with debris, polarimetric radars should provide V_R measurements within the debris field that have reduced variance compared to single-polarization weather radars. In addition, differential velocity V_D deviates appreciably from ± 2 m s^{-1} in RaXPol observations of the debris field. Locally enhanced magnitudes of V_D appear to be associated with relatively large σ_v and relatively low ρ_{hv}, indicating that

V_D may be an additional parameter useful for the detection of tornadic debris. If large magnitudes of V_D in tornado debris are associated with high σ_v, V_D may have an advantage over ρ_{hv} for the detection of ongoing tornadoes since ρ_{hv} can remain depressed after tornadoes have ended when the lofted debris is still settling (e.g., Ryzhkov et al. 2005; Schultz et al. 2012). Further examination of this quantity, particularly when calculated
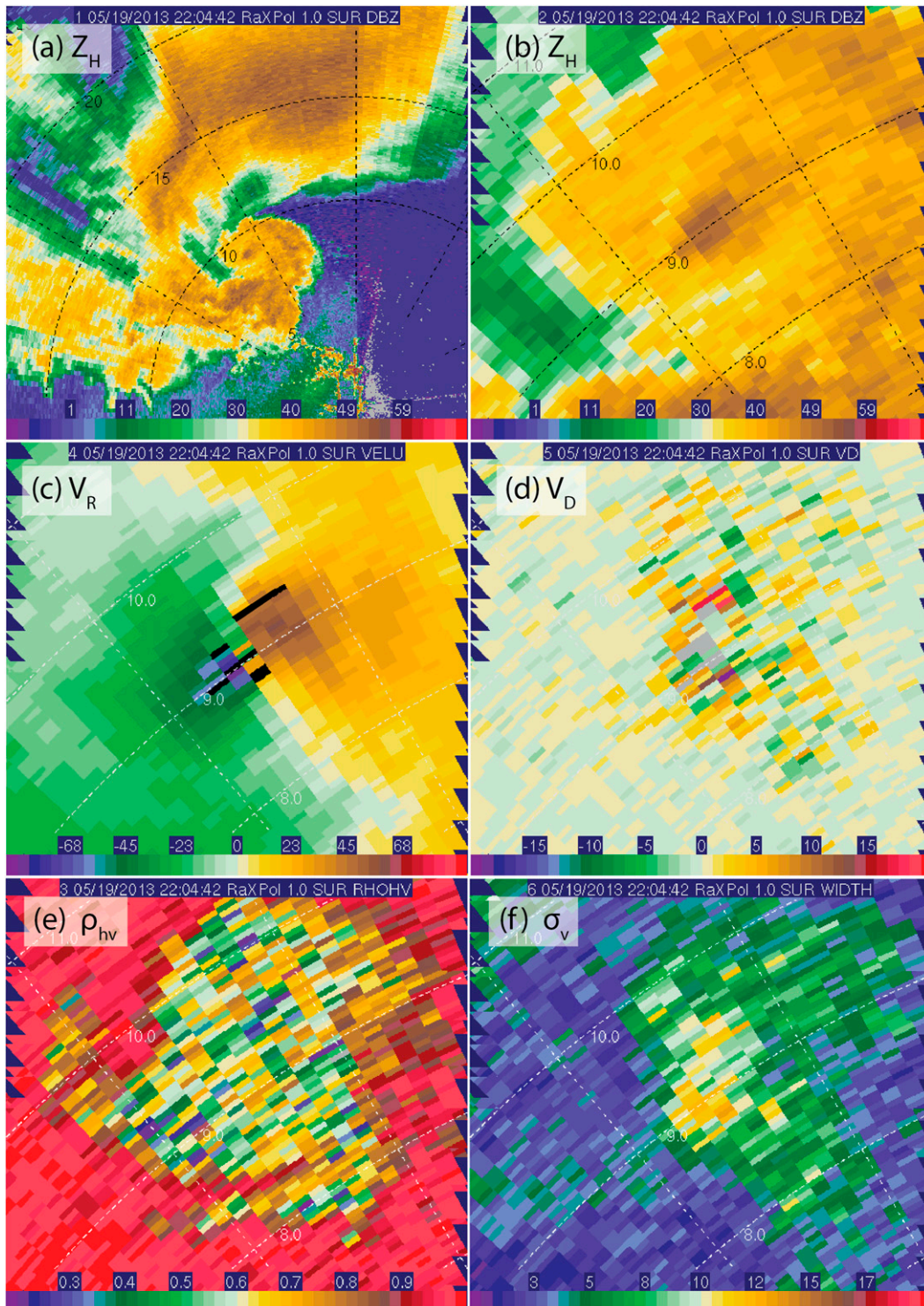
FIG. 19. RaXPol data valid at 2204:42 UTC 19 May 2013 south of Carney, OK: (a),(b) Z_H, (c) V_R, (d) V_D, (e) ρ_{hv}, and (f) σ_v. The maximum V_R is 90.9 m s^{-1} with an antenna boresight-aligned estimated beam height of ~103 m ARL. The elevation angle is 1°. Range rings are plotted every 5 km and spokes every 30° in (a); range rings are plotted every 1 km and spokes every 10° in (b)–(f).

using significantly more signal samples (e.g., 50+ pulse pairs per radial) to reduce statistical variability, seems warranted.

APPENDIX

Brief Review of Radar Quantities

The equivalent radar reflectivity factor at horizontal and vertical polarizations, ignoring attenuation, can be calculated as

$$Z_{h,v} = \frac{\lambda^4}{\pi^5 |K_w|^2} \int_0^\infty \sigma_{hh,vv}(D) N(D)\, dD$$
$$= \frac{4\lambda^4}{\pi^4 |K_w|^2} \int_0^\infty |f_{hh,vv}^{(b)}(D)|^2 N(D)\, dD \quad \text{and} \quad (A1a)$$

$$Z_{H,V} = 10\log(Z_{h,v}), \qquad (A1b)$$

where $Z_{h,v}$ is given in units of $mm^6\,m^{-3}$, $Z_{H,V}$ is given logarithmic units of dBZ, λ is the wavelength, $K_w = (m^2 - 1)/(m^2 + 2)$ is a dielectric factor of water (where m is the complex index of refraction), $\sigma_{hh,vv}(D)$ is the radar backscattering cross section at H and V polarization, $f_{hh,vv}^{(b)}(D)$ is the backward-scattering amplitudes at H and V polarization, and $N(D)$ is the drop-size (or particle-size) distribution (DSD). For spherical water hydrometeors with diameters $D < \lambda/16$, Z_H is proportional to D^6.

Differential reflectivity (e.g., Seliga and Bringi 1976) is usually given in units of decibels (dB) and is simply defined as

$$Z_{DR} = 10\log\left(\frac{Z_h}{Z_v}\right) = Z_H - Z_V. \qquad (A2)$$

In general, Z_{DR} is a measure of hydrometeor shape along the two polarization planes such that Z_{DR} increases from

near 0 dB for nearly spherical, small raindrops to several decibels for more oblate, larger raindrops. A distribution of randomly oriented scatterers of similar shape, size, and dielectric characteristic (e.g., tumbling hail) will tend to have $Z_{DR} \sim 0$ dB. Resonance effects that occur with non-Rayleigh scatterers can significantly complicate the interpretation of Z_{DR}.

The magnitude of the copolar cross-correlation coefficient at lag zero [i.e., $|\rho_{hv}(0)|$, or simply ρ_{hv}; Balakrishnan and Zrnić (1990)] can be defined as

$$|\rho_{hv}(0)| = \frac{\langle n f_{hh}^{(b)} f_{vv}^{(b)*} \rangle}{\langle n |f_{hh}^{(b)}|^2 \rangle^{1/2} \langle n |f_{vv}^{(b)}|^2 \rangle^{1/2}}, \qquad (A3)$$

where the asterisk (*) represents the complex conjugate operate and angle brackets ($\langle\ \rangle$) represent an ensemble mean of the enclosed quantity. In general, ρ_{hv} is a measure of the regularity of the shape, size, and dielectric characteristics of the scatterers within the radar volume. In rain, $\rho_{hv} \geq 0.98$ at common radar frequencies, and it generally decreases in areas of mixed-phased precipitation or hail (e.g., Balakrishnan and Zrnić 1990; Straka et al. 2000). In general, nonmeteorological scatterers such as biological scatterers (e.g., Zrnić and Ryzhkov 1999) and tornado debris (e.g., Ryzhkov et al. 2005; Bodine et al. 2013) are associated with $\rho_{hv} < 0.7$.

The specific propagation differential phase can be calculated from scattering amplitudes as

$$K_{DP} = \frac{180\lambda}{\pi} \int_0^\infty \text{Re}[f_{hh}^{(f)}(D) - f_{vv}^{(f)}(D)] N(D)\, dD, \quad (A4)$$

Where $f_{hh}^{(f)}(D)$ and $f_{vv}^{(f)}(D)$ are the H and V forward-scattering amplitudes and the term in the brackets following Re represents the real part of the difference. Typically, K_{DP} is calculated as the range derivative of differential phase (Φ_{DP}), although additional processing may be done to remove the effects of the backscatter differential phase from the total differential phase. In addition, K_{DP} tends to be insensitive to hail and is often used to estimate the rain rate based upon the proportionality between K_{DP} and liquid water content (e.g., Zrnić and Ryzhkov 1996).

REFERENCES

Alexander, C. R., and J. M. Wurman, 2008: Updated mobile radar climatology of supercell tornado structures and dynamics. *24th Conf. on Severe Local Storms,* Savannah, GA, Amer. Meteor. Soc., 19.4. [Available online at https://ams.confex.com/ams/24SLS/techprogram/paper_141821.htm-elevation.]

Asefi-Najafabady, S., K. Knupp, J. R. Mecikalski, R. M. Welch, and D. Phillips, 2010: Ground-based measurements and dual-Doppler

analysis of 3-D wind fields and atmospheric circulations induced by a meso-γ-scale inland lake. *J. Geophys. Res.,* **115,** D23117, doi:10.1029/2010JD014022.

Balakrishnan, N., and D. S. Zrnić, 1990: Use of polarization to characterize precipitation and discriminate large hail. *J. Atmos. Sci.,* **47,** 1525–1540, doi:10.1175/1520-0469(1990)047<1525: UOPTCP>2.0.CO;2.

Beamer, C. M., 1970: Measured antenna beam cross-section contours on a 230-km tropospheric scatter circuit. Collins Radio Company Internal Rep., 20 pp.

Beck, V., and N. Dotzek, 2010: Reconstruction of near-surface tornado wind fields from forest damage. *J. Appl. Meteor. Climatol.,* **49,** 1517–1537, doi:10.1175/2010JAMC2254.1.

Bluestein, H. B., and A. L. Pazmany, 2000: Observations of tornadoes and other convective phenomena with a mobile, 3-mm wavelength, Doppler radar: The Spring 1999 Field Experiment. *Bull. Amer. Meteor. Soc.,* **81,** 2939–2951, doi:10.1175/ 1520-0477(2000)081<2939:OOTAOC>2.3.CO;2.

——, J. G. LaDue, H. Stein, D. Speheger, and W. P. Unruh, 1993: Doppler radar wind spectra of supercell tornadoes. *Mon. Wea. Rev.,* **121,** 2200–2221, doi:10.1175/1520-0493(1993)121<2200: DRWSOS>2.0.CO;2.

——, M. M. French, R. L. Tanamachi, S. Frasier, K. Hardwick, F. Junyent, and A. L. Pazmany, 2007a: Close-range observations of tornadoes in supercells made with a dual-polarization, X-band, mobile Doppler radar. *Mon. Wea. Rev.,* **135,** 1522–1543, doi:10.1175/MWR3349.1.

——, C. C. Weiss, M. M. French, E. M. Holthaus, R. L. Tanamachi, S. Frasier, and A. L. Pazmany, 2007b: The structure of tornadoes near Attica, Kansas, on 12 May 2004: High-resolution mobile, Doppler radar observations. *Mon. Wea. Rev.,* **135,** 475–506, doi:10.1175/MWR3295.1.

——, M. M. French, I. PopStefanija, R. T. Bluth, and J. B. Knorr, 2010: A mobile, phased-array Doppler radar for the study of severe convective storms. *Bull. Amer. Meteor. Soc.,* **91,** 579–600, doi:10.1175/2009BAMS2914.1.

——, J. B. Houser, M. M. French, J. C. Snyder, G. D. Emmitt, I. PopStefanija, C. Baldi, and R. T. Bluth, 2014: Observations of the boundary layer near tornadoes and in supercells using a mobile, collocated, pulsed Doppler lidar and radar. *J. Atmos. Oceanic Technol.,* **31,** 302–325, doi:10.1175/ JTECH-D-13-00112.1.

Bodine, D. J., M. R. Kumjian, R. D. Palmer, P. L. Heinselman, and A. V. Ryzhkov, 2013: Tornado damage estimation using polarimetric radar. *Wea. Forecasting,* **28,** 139–158, doi:10.1175/ WAF-D-11-00158.1.

Brooks, H. E., 2004: On the relationship of tornado path length and width to intensity. *Wea. Forecasting,* **19,** 310–319, doi:10.1175/ 1520-0434(2004)019<0310:OTROTP>2.0.CO;2.

——, and C. A. Doswell III, 2001: Some aspects of the international climatology of tornadoes by damage classification. *Atmos. Res.,* **56,** 191–201, doi:10.1016/S0169-8095(00)00098-3.

——, J. W. Lee, and J. P. Craven, 2003: The spatial distribution of severe thunderstorm and tornado environments from global reanalysis data. *Atmos. Res.,* **67–68,** 73–94, doi:10.1016/ S0169-8095(03)00045-0.

Dolan, B., and S. A. Rutledge, 2009: A theory-based hydrometeor identification algorithm for X-band polarimetric radars. *J. Atmos. Oceanic Technol.,* **26,** 2071–2088, doi:10.1175/ 2009JTECHA1208.1.

Doswell, C. A., III, H. Brooks, and N. Dotzek, 2009: On the implementation of the enhanced Fujita scale in the USA. *Atmos. Res.,* **93,** 554–563, doi:10.1016/j.atmosres.2008.11.003.

Doviak, R. J., and D. S. Zrnić, 1993: *Doppler Radar and Weather Observations.* 2nd. ed. Academic Press, 562 pp.

Dowell, D. C., C. R. Alexander, J. M. Wurman, and L. J. Wicker, 2005: Centrifuging of hydrometeors and debris in tornadoes: Radar-reflectivity patterns and wind-measurement errors. *Mon. Wea. Rev.,* **133,** 1501–1524, doi:10.1175/ MWR2934.1.

Edwards, R., J. G. LaDue, J. T. Ferree, K. Scharfenberg, C. Maier, and W. L. Coulbourne, 2013: Tornado intensity estimation: Past, present, and future. *Bull. Amer. Meteor. Soc.,* **94,** 641–653, doi:10.1175/BAMS-D-11-00006.1.

Federal Emergency Management Agency, 2012: Spring 2011 tornadoes: April 25–28 and May 22. FEMA Mitigation Assessment Team Rep. FEMA P-908, 512 pp.

Fiedler, B. H., and R. Rotunno, 1986: A theory for the maximum wind speeds in tornado-like vortices. *J. Atmos. Sci.,* **43,** 2328–2340, doi:10.1175/1520-0469(1986)043<2328: ATOTMW>2.0.CO;2.

French, M. M., L. J. Wicker, D. W. Burgess, and E. R. Mansell, 2013: Mobile, Doppler polarimetric radar observations of supercell hook echoes during VORTEX2. *36th Conf. on Radar Meteorology,* Breckenridge, CO, Amer. Meteor. Soc., 13A.4. [Available online at https://ams.confex.com/ams/36Radar/ webprogram/Paper228657.html.]

Fujita, T. T., 1981: Tornadoes and downbursts in the context of generalized planetary scales. *J. Atmos. Sci.,* **38,** 1511–1534, doi:10.1175/1520-0469(1981)038<1511:TADITC>2.0.CO;2.

Garner, J. M., 2012: Environments of signature tornadoes occurring with the warm sector versus those occurring along surface baroclinic boundaries. *Electron. J. Severe Storms Meteor.,* **7** (5). [Available online at http://ejssm.org/ojs/index.php/ejssm/ issue/view/38.]

Gong, B., D. C. Lewellen, and W. S. Lewellen, 2006: The effects of fine-scale debris on different tornado corner flows. *23rd Conf. on Severe Local Storms,* St. Louis, MO, Amer. Meteor. Soc., P10.3. [Available online at http://ams.confex.com/ams/pdfpapers/ 115317.pdf.]

Houser, J. B., 2013: Rapid-scan, polarimetric, Doppler radar observations of supercell tornado evolution on 24 May 2011. Ph.D. dissertation, University of Oklahoma, 264 pp.

Karstens, C. D., W. A. Gallus, B. D. Lee, and C. A. Finley, 2013: Analysis of tornado-induced tree fall using aerial photography from the Joplin, Missouri, and Tuscaloosa–Birmingham, Alabama, tornadoes of 2011. *J. Appl. Meteor. Climatol.,* **52,** 1049–1068, doi:10.1175/JAMC-D-12-0206.1.

Kerr, B. W., and G. L. Darkow, 1996: Storm-relative winds and helicity in the tornadic thunderstorm environment. *Wea. Forecasting,* **11,** 489–505, doi:10.1175/1520-0434(1996)011<0489: SRWAHI>2.0.CO;2.

Kosiba, K. A., and J. Wurman, 2013: The three-dimensional structure and evolution of a tornado boundary layer. *Wea. Forecasting,* **28,** 1552–1561, doi:10.1175/WAF-D-13-00070.1.

Kuligowski, E. D., F. T. Lombardo, L. T. Phan, M. L. Levitan, and D. P. Jorgensen, 2013: Technical investigation of the May 22, 2011, tornado in Joplin, Missouri. Draft Final Rep. NIST NCSTAR 3, National Institute of Standards and Technology, 428 pp.

Kumjian, M. R., 2011: Precipitation properties of supercell hook echoes. *Electron. J. Severe Storms Meteor.,* **6** (5). [Available online at http://ejssm.org/ojs/index.php/ejssm/issue/view/30.]

——, and A. V. Ryzhkov, 2008: Polarimetric signatures in supercell thunderstorms. *J. Appl. Meteor. Climatol.,* **47,** 1940–1961, doi:10.1175/2007JAMC1874.1.

Lewellen, D. C., and W. S. Lewellen, 2007: Near-surface intensification of tornado vortices. *J. Atmos. Sci.,* **64,** 2176–2194, doi:10.1175/JAS3965.1.

——, B. Gong, and W. S. Lewellen, 2008: Effects of finescale debris on near-surface tornado dynamics. *J. Atmos. Sci.,* **65,** 3247–3262, doi:10.1175/2008JAS2686.1.

Lewellen, W. S., J. Xia, and D. C. Lewellen, 2002: Transonic velocities in tornadoes? Preprints, *21st Conf. on Severe Local Storms,* San Antonio, TX, Amer. Meteor. Soc., P10.2. [Available online at https://ams.confex.com/ams/pdfpapers/46933.pdf.]

Mead, C. M., and R. L. Thompson, 2011: Environmental characteristics associated with nocturnal significant-tornado events in the central and southern Great Plains. *Electron. J. Severe Storms Meteor.,* **6** (6). [Available online at http://www.ejssm.org/ojs/index.php/ejssm/article/viewArticle/84.]

Melnikov, V. M., 2004: Simultaneous transmission mode for the polarimetric WSR-88D: Statistical biases and standard deviations of polarimetric variables. NOAA/NSSL Rep., 84 pp.

——, and D. S. Zrnić, 2004: Estimates of large spectrum width from autocovariances. *J. Atmos. Oceanic Technol.,* **21,** 969–974, doi:10.1175/1520-0426(2004)021<0969:EOLSWF>2.0.CO;2.

——, ——, A. Ryzhkov, A. Zahrai, and J. Carter, 2009: Validation of attenuation correction at X band performed with collocated S-band polarimetric radar. *34th Conf. on Radar Meteorology,* Williamsburg, VA, Amer. Meteor. Soc., 11A.5. [Available online at https://ams.confex.com/ams/pdfpapers/155322.pdf.]

——, M. Leskinen, and J. Koistinen, 2014: Doppler velocities at orthogonal polarizations in radar echoes from insects and birds. *IEEE Geosci. Remote Sens. Lett.,* **11,** 592–596, doi:10.1109/LGRS.2013.2272011.

Nolan, D. S., 2013: On the use of Doppler radar–derived wind fields to diagnose the secondary circulations of tornadoes. *J. Atmos. Sci.,* **70,** 1160–1171, doi:10.1175/JAS-D-12-0200.1.

Park, H., A. V. Ryzhkov, D. S. Zrnić, and K. Kim, 2009: The hydrometeor classification algorithm for the polarimetric WSR-88D: Description and application to an MCS. *Wea. Forecasting,* **24,** 730–748, doi:10.1175/2008WAF2222205.1.

Pazmany, A. L., J. B. Mead, H. B. Bluestein, J. C. Snyder, and J. B. Houser, 2013: A mobile rapid-scanning polarimetric (RaXPol) Doppler radar system. *J. Atmos. Oceanic Technol.,* **30,** 1398–1413, doi:10.1175/JTECH-D-12-00166.1.

Rotunno, R., 1979: A study in tornado-like vortex dynamics. *J. Atmos. Sci.,* **36,** 140–155, doi:10.1175/1520-0469(1979)036<0140:ASITLV>2.0.CO;2.

——, 2013: The fluid dynamics of tornadoes. *Annu. Rev. Fluid Mech.,* **45,** 59–84, doi:10.1146/annurev-fluid-011212-140639.

Ryzhkov, A. V., 2007: The impact of beam broadening on the quality of radar polarimetric data. *J. Atmos. Oceanic Technol.,* **24,** 729–744, doi:10.1175/JTECH2003.1.

——, T. J. Schuur, D. W. Burgess, and D. S. Zrnić, 2005: Polarimetric tornado detection. *J. Appl. Meteor.,* **44,** 557–570, doi:10.1175/JAM2235.1.

Schultz, C. J., and Coauthors, 2012: Dual-polarization tornadic debris signatures, part I: Examples and utility in an operational setting. *Electron. J. Oper. Meteor.,* **13,** 120–137.

Seliga, T. A., and V. N. Bringi, 1976: Potential use of radar differential reflectivity measurements at orthogonal polarizations for measuring precipitation. *J. Appl. Meteor.,* **15,** 69–76, doi:10.1175/1520-0450(1976)015<0069:PUORDR>2.0.CO;2.

Snyder, J. C., H. B. Bluestein, G. Zhang, and S. J. Frasier, 2010: Attenuation correction and hydrometeor classification of

high-resolution, X-band, dual-polarized mobile radar measurements in severe convective storms. *J. Atmos. Oceanic Technol.,* **27,** 1979–2001, doi:10.1175/2010JTECHA1356.1.

——, ——, V. Venkatesh, and S. J. Frasier, 2013: Observations of polarimetric signatures in supercells by an X-band mobile Doppler radar. *Mon. Wea. Rev.,* **141,** 3–29, doi:10.1175/MWR-D-12-00068.1.

Straka, J. M., D. S. Zrnić, and A. V. Ryzhkov, 2000: Bulk hydrometeor classification and quantification using polarimetric radar data: Synthesis of relations. *J. Appl. Meteor.,* **39,** 1341–1372, doi:10.1175/1520-0450(2000)039<1341:BHCAQU>2.0.CO;2.

Testud, J., E. Le Bouar, E. Obligis, and M. Ali-Mehenni, 2000: The rain profiling algorithm applied to polarimetric weather radar. *J. Atmos. Oceanic Technol.,* **17,** 332–356, doi:10.1175/1520-0426(2000)017<0332:TRPAAT>2.0.CO;2.

Thampi, H., V. Dayal, and P. P. Sarkar, 2011: Finite element analysis of interaction of tornados with low-rise timber building. *J. Wind Eng. Ind. Aerodyn.,* **99,** 369–377, doi:10.1016/j.jweia.2011.01.004.

Thompson, R. L., R. Edwards, J. A. Hart, K. L. Elmore, and P. M. Markowski, 2003: Close proximity soundings within supercell environments obtained from the Rapid Update Cycle. *Wea. Forecasting,* **18,** 1243–1261, doi:10.1175/1520-0434(2003)018<1243:CPSWSE>2.0.CO;2.

——, C. M. Mead, and R. Edwards, 2007: Effective storm-relative helicity and bulk shear in supercell thunderstorm environments. *Wea. Forecasting,* **22,** 102–115, doi:10.1175/WAF969.1.

Wakimoto, R. M., P. Stauffer, W.-C. Lee, N. T. Atkins, and J. Wurman, 2012: Finescale structure of the LaGrange, Wyoming, tornado during VORTEX2: GBVTD and photogrammetric analyses. *Mon. Wea. Rev.,* **140,** 3397–3418, doi:10.1175/MWR-D-12-00036.1.

Weiss, C. C., J. L. Schroeder, J. Guynes, A. E. Reinhart, P. S. Skinner, and S. Gunter, 2011: A review of Texas Tech Ka-band operations during VORTEX2. *35th Conf. on Radar Meteorology,* Pittsburgh, PA, Amer. Meteor. Soc., 7B.2. [Available online at https://ams.confex.com/ams/35Radar/webprogram/Paper191783.html.]

Womble, J. A., and D. A. Smith, 2009: Common misconceptions in determining wind/water damage causation. *Proc. 2009 Structures Conf.,* Austin, TX, Structural Engineering Institute of the American Society of Civil Engineers, 1307–1316.

——, ——, K. Mehta, and J. McDonald, 2009: The enhanced Fujita scale: For use beyond tornadoes? *Proc. Fifth Forensic Engineering Conf.,* Washington, DC, Technical Council on Forensic Engineering of the American Society of Civil Engineers, 699–708.

——, ——, J. McDonald, and K. Mehta, 2011: Intended use and potential misuse of the EF scale. *11th Americas Conf. on Wind Engineering,* San Juan, PR, International Association for Wind Engineering. [Available at http://www.iawe.org/Proceedings/11ACWE/11ACWE-Womble1.pdf.]

WSEC, 2006: A recommendation for an enhanced Fujita scale (EF-scale). Wind Science and Engineering Center Rep., Texas Tech University, 108 pp. [Available online at http://www.depts.ttu.edu/nwi/Pubs/FScale/EFScale.pdf.]

Wurman, J., and C. Alexander, 2005: The 30 May 1998 Spencer, South Dakota. storm. Part II: Comparison of observed damage and radar-derived winds in the supercell tornadoes. *Mon. Wea. Rev.,* **133,** 97–119, doi:10.1175/MWR-2856.1.

——, J. Straka, E. Rasmussen, M. Randall, and A. Zahrai, 1997: Design and deployment of a portable, pencil-beam, pulsed,

3-cm Doppler radar. *J. Atmos. Oceanic Technol.,* **14,** 1502–1512, doi:10.1175/1520-0426(1997)014<1502:DADOAP>2.0.CO;2.

——, C. Alexander, P. Robinson, and Y. Richardson, 2007: Low-level winds in tornadoes and potential catastrophic tornado impacts in urban areas. *Bull. Amer. Meteor. Soc.,* **88,** 31–46, doi:10.1175/BAMS-88-1-31.

——, K. Kosiba, and P. Robinson, 2013: In situ, Doppler radar, and video observations of the interior structure of a tornado and the wind–damage relationship. *Bull. Amer. Meteor. Soc.,* **94,** 835–846, doi:10.1175/BAMS-D-12-00114.1.

——, ——, ——, and T. Marshall, 2014: The role of multiple vortex tornado structure in causing storm researcher fatalities. *Bull. Amer. Meteor. Soc.,* **95,** 31–45, doi:10.1175/BAMS-D-13-00221.1.

Xia, J., W. S. Lewellen, and D. C. Lewellen, 2003: Influence of Mach number on tornado corner flow dynamics. *J. Atmos. Sci.,* **60,** 2820–2825, doi:10.1175/1520-0469(2003)060<2820:IOMNOT>2.0.CO;2.

Zrnić, D. S., 1977: Spectrum width estimates from correlated pulse pairs. *IEEE Trans. Aerosp. Electron. Syst.,* **AES-13,** 344–354, doi:10.1109/TAES.1977.308467.

——, and A. V. Ryzhkov, 1996: Advantages of rain measurements using specific differential phase. *J. Atmos. Oceanic Technol.,* **13,** 454–464, doi:10.1175/1520-0426(1996)013<0454:AORMUS>2.0.CO;2.

——, and ——, 1999: Polarimetry for weather surveillance radars. *Bull. Amer. Meteor. Soc.,* **80,** 389–406, doi:10.1175/1520-0477(1999)080<0389:PFWSR>2.0.CO;2.